Examination and Development of RF inductors by using the Finite Element Method

by

Zoltán Pólik
B.Sc. student in Electrical Engineering

supervisor

Dr. Miklós Kuczmann, Ph.D.
Associate Professor

A thesis submitted to the
Széchenyi István University
for the degree of
B.Sc. in Electrical Engineering

Department of Telecommunication
Laboratory of Electromagnetic Fields
Széchenyi István University
Győr
2008

Diplomaterv feladat kiírás

Pólik Zoltán
B.Sc. hallgató

távközlési informatika szakirányos hallgató részére

A diplomaterv címe:

Examination and Development of RF Inductors by using the Finite Element Method

RF Induktivitások Vizsgálata és Fejlesztése Végeselem-módszerrel

A diplomaterv feladat kiírása:
A végeselem-módszer alkalmazása rádiófrekvencián működő induktivitások vizsgálatában és fejlesztésében. A feladat megoldásához szükséges potenciálformalizmus leírása és végeselemes modellbe való beillesztése. Az alkatrész modellezése két- és háromdimenziós modellel. A gyártóval közösen kidolgozott szisztéma alapján a modell módosítása és a módosítások hatásának vizsgálata a felépített modell segítségével. A szimulációs eredmények összevetése mérési eredményekkel. Az alkatrész lehetséges fejlesztési irányainak meghatározása.

2008. október 4.

Konzulens:

Dr. Kuczmann Miklós, PhD
egyetemi docens
Távközlési Tanszék

Pólik Zoltán

Announcement of the BSc Thesis

Zoltán Pólik
B.Sc. student

Student of Department of Telecommunication

Title of the Thesis:

Examination and Development of RF Inductors by using the Finite Element Method

Announcement of the BSc Thesis:
Applying the finite element method in examination and development of inductors, which work in the range of the radio frequency. Determination of the potential formulation for the solution of the problem and the building of it into a finite element model. The two and the three dimensional modeling of the component. The modification of the component and the examination of the effects of the modifications by using the realized model according to the method, which is described by the help of the manufacturer. The comparison of the results of the simulations and the measurements. The determination of the possible orientation of the development of the component.

4^{th} of October 2008.

Supervisor:

Dr. Miklós Kuczmann, PhD
Associate Professor
Department of Telecommunication

Zoltán Pólik

Contents

Chapter 1

Introduction

An inductor is a passive electronic component, which stores magnetic energy [1]. The most simple realization of it consists of a wire loop, but there are inductors having some thousands of turns. The winding of the component may surround solenoidal, toroidal and any other various shaped cores made of ferromagnetic or dielectric materials. Inductors can be purchased in many various sizes depending on the sphere of operation.

In the case of a theoretical inductor, the relationship between the time-varying voltage u_L of the component and the time-varying current i_L passing through is described by the following differential equation [2]:

$$u_L(t) = L\frac{\mathrm{d}i_L(t)}{\mathrm{d}t}. \tag{1.1}$$

The term inductance denoted by L was coined by Oliver Heaviside in February, 1886. In honour of Joseph Henry, the unit of inductance has been given the name henry [H]. 1 H= $\frac{1\mathrm{Wb}}{\mathrm{A}}$. In SI base units, the dimensions of the weber are $\frac{\mathrm{kg\,m^2}}{\mathrm{s^2\,A}}$. In derived units, they are volt-seconds (Vs). The ratio of the magnetic flux Φ to the current i_L is called the self-inductance, which is usually referred to as the inductance of the component. In general, the expression of the self-inductance is [3, 4]

$$L = N\frac{\Phi}{i_L}, \tag{1.2}$$

where N is the number of turns.

An ideal inductor has inductance, but it has not got resistance and capacitance and it does not dissipate energy, however it can not be manufactured. The real inductor has series resistance caused by the resistance of the winding wire, which is usually made of copper and it has some capacitance due to the distributed capacitance between the turns of the wire, moreover it dissipates energy in the resistance of the wire. Magnetic core inductors may dissipate energy in the core due to hysteresis, too. This is the reason why the inductor is the least ideal passive electronic component and it is one of the most difficult one to model.

Electronic component manufacturers spend much time and money to develop their inductors and to improve their attributes such as the value of the inductance, the impedance, the quality factor, the dimensions of the components, etc. Nowadays, in the development stage the most prevalent method is still based on the analytical and on the experimental results. Manufacturers construct many trial components and than they

examine the effects of the modifications. To the modifications they invoke the works of radio amateurs who worked in the beginning of the last century such as Nagaoka, Medhurst, Lundin, Wheeler, etc [5–8]. After all, CAD (Computer Aided Design) is more and more popular in research, developing and manufacturing new components, because of its speed, simplicity and practicability.

The aim of my research is to help the EPCOS AG in examining, developing and designing inductors by using the finite element method.

1.1 The Scope of my Work

The scope of my degree work is to simulate SMT inductors by using the finite element method, to draw the inference of the simulations and to develop some attributes to improve the components.

In my personal point of view the most important goal of my study is to understand the interior working of inductors, which depends on several physical phenomena, to understand the effect of these phenomena to the attributes of the component and to realize how to modify the important attributes of the inductors through modifying some specialities.

In engineering point of view the aim of the research is to build up a finite element model to simulate inductors accurately, which model have to predict both of the important attributes of inductors, such as inductance, impedance, resistance, quality factor, in the whole range of the frequency. After that we can be in possession of the knowledge with which better inductors can be designed.

To realize the above ambitions, first of all a finite element model is built up, which is able to simulate inductors with various sizes, geometries and materials. During this work the vector finite element model and has been used, where potential formulations based on the magnetic vector potential $\boldsymbol{A}$ and the electric scalar potential V have been applied. A method has been worked out to set the results of the simulation to the measured data of the modeled inductor, towards the exact predicting of the attributes.

To increase the quality factor of the examined inductor, several modifications in the coil of the component have been tried out in simulation and in manufacturing. To check the correctness of the model several trial components have been manufactured and the measurements of these components have been done in the laboratory of the manufacturer, in Szombathely, Hungary, moreover the measured and the simulated data have been compared.

Finally, a recommendation about the further improvement of the examined inductor is sent to the manufacturer.

In an earlier challenge a three dimensional finite element model was worked out to simulate the variation of the inductance as a function of a manufacturing failure and the orientation of the eddy currents inside the component. The building up and the results of this simulation will be also presented briefly in this thesis.

The organization of my work is the following.

Chapter 2 contains a brief overview of some results known from the literature. The basic important attributes of inductors, some results of the works of radio amateurs at the beginning of the 20^{th} century, a way to modeling inductors analytically and some information about the finite element method can be found there.

The following chapters contain the summary of my research activity.

In chapter 3, the theoretical background of the realized simulations has been described. The starting point is Maxwell's equation system, from which the used potential formulations can be deduced. The finite element method is based on the weak formulation of the potential formulations, so this chapter presents the deduction of the weak formulation applying mathematical rules and methods.

Chapter 4 presents the simulation of inductors in the COMSOL Multiphysics software package. The overviews of the problems, the building up of the finite element models, the simulations, the computational results and the comparison of the measured and the simulated data can be found there step by step.

Last, the conclusions of my work with future works can be found in chapter 5. The main references of my research are also given at the end of this paper.

To write this document the LaTeX word processor have been used.

1.2 Acknowledgment

This paper was supported by Széchenyi István University (15-3210-02), by the EPCOS AG, by the Hungarian Scientific Research Fund (OTKA PD 73242) and by the János Bolyai Research Scholarship of the Hungarian Academy of Sciences (BO/00064/06)

I wish to express my grateful acknowledgement to my supervisor Dr. Miklós Kuczmann, Ph.D. for his advices, encouragements and suggestions provided my studies and of his assistance during developing the finite models. I am very grateful to György Novotny and Péter Csurgai for their assistance during manufacturing and measuring trial components and for their acceptance of my ideas in developing. I would like to thank the members of the Laboratory of Electromagnetic Fields and last but not least, I would like to thank my family and my friends for the daily assistance and patience.

Chapter 2

Literature Overview

2.1 Important Attributes of Inductors

During the design of inductors, there are several attributes, which are needed to consider according to the field of application.

In the case of inductors the most important attribute is the inductance, which has been determined in chapter 1. However, the presented formula is not useful to simulate and to measure real inductors, because they have resistance – represents the resistance of the coil – in series with the inductance. In parallel the inductance and the resistance the real inductor has capacitance – which represent the distributed capacitance between the turns. This is the simplest model of an inductor, which can be seen in Fig. 2.1.

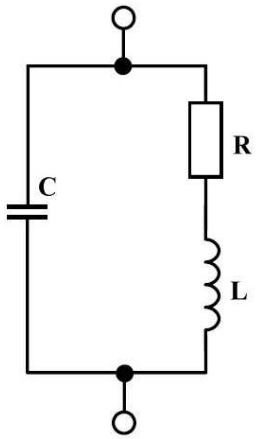

Fig. 2.1. The simplest three element model of a real inductor

The inductance of a real inductor can be determined from the equivalent impedance $\bar{Z}_L$ of it. The equivalent impedance is the extension of the Ohm's law in the case of AC circuits, in other words, it means the complex amplitude of sinusoidal voltage

$$\hat{\bar{U}} = \hat{U}\mathrm{e}^{\mathrm{j}(\omega t+\varphi_U)} \tag{2.1}$$

divided by the complex amplitude of sinusoidal current

$$\hat{\bar{I}} = \hat{I}\mathrm{e}^{\mathrm{j}(\omega t+\varphi_I)} \tag{2.2}$$

passing through it, where ω is the angular frequency, and $\omega = 2\pi f$, where f is the frequency, moreover $\hat{U}$ is the peak value of the voltage, $\hat{I}$ is the peak value of the current, t is the time and φ_U is the phase of the voltage and φ_I is the phase of the current. Dimensionally, impedance is the same as resistance, so the SI unit of it is [Ω],

$$\bar{Z}_L = Z_L \mathrm{e}^{\mathrm{j}\theta} = \frac{\hat{\bar{U}}}{\hat{\bar{I}}}, \tag{2.3}$$

where $\bar{Z}_L$ is the complex impedance and $\theta = \varphi_U - \varphi_I$. The above expression results in a complex number, so the equivalent impedance of a component or a circuit is not only depends on the amplitudes of the voltage and current, but it also depends on the phases. It can also be described by the following formula, as well:

$$\bar{Z}_L = R + \mathrm{j}X, \tag{2.4}$$

where the real part of the impedance is the resistance R, and the imaginary part X is called reactance. The reactance of an inductor and a capacitor can be described by

$$X_L = 2\pi f L \tag{2.5}$$

and

$$X_C = \frac{1}{2\pi f C}. \tag{2.6}$$

The determination of the equivalent series inductance L_s of an inductor is coming from (2.4). During measurements and simulations the following expression has been used to determine the equivalent inductance of the components:

$$L_s = \frac{\mathfrak{Im}\{\bar{Z}_L\}}{2\pi f}. \tag{2.7}$$

It seems that L_s contains the inductive and the capacitive parts of the reactance, too, but the effect of the capacitance become significant only at high frequencies, around the SRF and above (self resonant frequency) denoted by f_0.

SRF is the frequency where the inductive reactance and the capacitive reactance are equal in magnitude causing electrical energy to oscillate between the magnetic field of the inductive part and the electric field of the capacitive part of the component. At resonance, the series impedance of the capacitance and the inductance is minimal, i.e. it is equal to zero, and the parallel impedance of the components is maximal. Since the inductive reactance and the capacitive reactance are of equal magnitude, $\omega L = \frac{1}{\omega C}$ can be written, so [2, 9, 10]

$$\omega_0 = \frac{1}{\sqrt{LC}}, \tag{2.8}$$

which is also called Thomson equation, where is $\omega_0 = 2\pi f_0$, and f_0 is the self-resonance frequency.

In the case of RF inductors one of the most important attributes is the quality factor Q. In physics and engineering, the quality factor, or Q-factor is a dimensionless parameter that compares the time constant for decay of an oscillating physical system's amplitude to its oscillation period. Equivalently, it compares the frequency at which a system oscillates to the rate at which it dissipates its energy [2,10]. A higher Q indicates

a lower rate of energy dissipation relative to the oscillation frequency, so the oscillations die out slower. For example, in electronics, high quality factor desires in a good tuned circuit or resonator. Generally, Q is defined by [10]

$$Q = \omega \frac{E_S}{P_L}, \tag{2.9}$$

where E_S is the stored energy and P_L is the power loss. Because $P_L = \frac{W_C}{t}$, where W_C is the energy dissipated per cycle, (2.9) can be reformed, which results in

$$Q = 2\pi \frac{E_S}{W_C}. \tag{2.10}$$

For a complex impedance, such as an inductor, the Q-factor is the ratio of the reactance to the resistance, i.e.

$$Q = \frac{|\mathfrak{Im}\{\bar{Z}\}|}{\mathfrak{Re}\{\bar{Z}\}}. \tag{2.11}$$

It can also be calculated by knowing only the power factor PF

$$Q = \frac{\sqrt{1 - PF^2}}{PF} = \sqrt{\frac{1}{PF^2} - 1}, \tag{2.12}$$

where PF is the ratio of the real power to the apparent power. The quality factor can be calculated, by using the following formula, too,

$$Q = \frac{|sin\phi|}{|cos\phi|} = |tan\phi|, \tag{2.13}$$

where ϕ is the phase anlge of the complex impedance.

2.2 Works of Radio Amateurs

At the beginning of the 20^{th} century the wireless communication became a world-wide hobby and entertainment. People who use various types of radio communication equipments to communicate with other ones for public service, recreation and self-training are called radio amateurs. The term amateur is not a reflection on the skills of the participants, who are often quite advanced. Rather, amateur indicates that amateur radio communications are not allowed to be made for commercial or money-making purposes.

Several radio amateurs were interested in developing radios and their components. Many papers was published about inductors, antennas and all kinds of wireless applications and its behaviors [4–7]. In the case of inductors we can read several articles about the calculation of high frequency resistance, self-capacitance, self- and mutual inductance, and studies about the skin effect, the closely and widely spaced coils and so on [7, 8].

The one of the first and the most important papers is written by Nagaoka, which title is *The Inductance Coefficients of Solenoids* [5]. The most relevant aim of his research was to find a standard formula to the accurate calculation of the self-inductance and the mutual inductance of solenoidal shaped inductors. In the case of my degree work, only the part of the calculation of the self-inductance is important, so only this part of his work will be shown in this paper.

The reason of his research was, that several formula have been deduced before to calculate the self-inductance of solenoids by different physicists. They determined different forms according to the length of the solenoid was short or long. Most of them werw quite complicated and not suitable for engineers or physicists. Nagaoka deduced a new universal formula to calculate the self-inductance of a solenoid easily by tabulating a certain coefficient $\mathfrak{L}$, which is nowadays marked with K and named Nagaoka coefficient or Nagaoka constant [5]. Basically, the self-inductance of an infinite long solenoid is given by [5]

$$L = \frac{\mu_0 N^2 A}{l}, \tag{2.14}$$

where $\mu_0 = 4\pi\, 10^{-7}\, \frac{\mathrm{H}}{\mathrm{m}}$, which is the permeability of free space, N is the number of turns, A is the cross-section area of the coil and l is the length of the coil. The inductance of a single layer solenoid with any length can be calculated by using the following formula,

$$L = \frac{\mu_0 N^2 A}{l} K, \tag{2.15}$$

where K is the Nagaoka constant, which is the function of diameter per length [5]. He created a lot of tables to calculate K; the most obvious one gives the value of K from the constant $\frac{Diameter}{Length}$. A part of Nagaoka's table can be seen in Fig. 2.2.

The necessity of Nagaoka coefficient is explicable by the non-uniformity of the magnetic field inside the inductor. In 1911, Edward B. Rosa and Frederick W. Grover summarized all of the expressions and tables on calculation the mutual- and self-inductances determined by Maxwell, Nagaoka, Havelock, Rayleigh, Lorenz, etc. in the book *Formulas and Tables for the Calculation of Mutual and Self-induction* [8].

Afterwards, people wanted to recognize the behavior of inductors more and more precisely. In the middle of the 20^{th} century some papers have been written about the resistance, the self-capacitance, the self resonance frequency, the skin effect and the proximity effect by physicists and engineers, such as Butterworth and Medhurst [7]. They described the behavior of the variation of self-capacitance, and via it, the variation of the SRF as a function of the diameter of the coil. For example, they discovered that if the diameter of the wire is increasing, the self-capacitance of the inductor is also increasing, but the inductance of the component is decreasing; and if the distance between the adjacent wire centers is increasing, the self-capacitance and the inductance of the inductor are decreasing [7]. They explained why the resistance of an inductor, which has several turns, is modified in the context of the frequency, the wire diameter and the distance between the adjacent wires. In the case of an isolated wire, the exciting current is distributed uniformly throughout the material at low frequencies. At high frequencies the current is flowing in a thin layer close to the surface. This is the skin effect [11]. In coiled-wire inductors, the skin effect is modified not only by the conductivity of the material σ, but by an interaction with the external magnetic field. This phenomenon is known as the proximity effect [11]. The proximity effect is the reason of that the resistance of an inductor with "closely-spaced" turns is greater than in the case of "widely-spaced" coils, because the flowing current in a wire is more and more crowded out by the magnetic field of an adjacent wire [7, 12]. An example for the proximity effect can be seen in Fig. 2.3. The figure shows the total current density in the coil simulated by FEM.

Diameter / Length	$\mathfrak{L}$	Δ_1	Diameter / Length	$\mathfrak{L}$	Δ_1
0·60	0·788 525	−0·002 850	**0·95**	0·699 509	−0·002 247
0·61	0·785 675	−0·002 831	**0·96**	0·697 262	−0·002 232
0·62	0·782 844	−0·002 812	**0·97**	0·695 030	−0·002 217
0·63	0·780 032	−0·002 792	**0·98**	0·692 813	−0·002 202
0·64	0·777 240	−0·002 773	**0·99**	0·690 611	−0·002 188
0·65	0·774 467	−0·002 754	**1·00**	0·688 423	−0·010 726
0·66	0·771 713	−0·002 735	**1·05**	0·677 697	−0·010 382
0·67	0·768 978	−0·002 716	**1·10**	0·667 315	−0·010 052
0·68	0·766 262	−0·002 697	**1·15**	0·657 263	−0·009 736
0·69	0·763 565	−0·002 679	**1·20**	0·647 527	−0·009 432
0·70	0·760 886	−0·002 661	**1·25**	0·638 095	−0·009 145
0·71	0·758 225	−0·002 643	**1·30**	0·628 950	−0·008 864
0·72	0·755 582	−0·002 624	**1·35**	0·620 086	−0·008 599
0·73	0·752 958	−0·002 607	**1·40**	0·611 487	−0·008 343
0·74	0·750 351	−0·002 589	**1·45**	0·603 144	−0·008 099
0·75	0·747 762	−0·092 571	**1·50**	0·595 045	−0·007 863
0·76	0·745 191	−0·002 554	**1·55**	0·587 182	−0·007 639
0·77	0·742 637	−0·002 537	**1·60**	0·579 543	−0·007 424
0·78	0·740 100	−0·002 519	**1·65**	0·572 119	−0·007 216
0·79	0·737 581	−0·002 502	**1·70**	0·564 903	−0·007 018
0·80	0·735 079	−0·002 486	**1·75**	0·557 885	−0·006 828
0·81	0·732 593	−0·002 467	**1·80**	0·551 057	−0·006 644
0·82	0·730 126	−0·002 451	**1·85**	0·544 413	−0·006 468
0·83	0·727 675	−0·002 435	**1·90**	0·537 945	−0·006 298
0·84	0·725 240	−0·002 419	**1·95**	0·531 647	−0·006 137
0·85	0·722 821	−0·002 402	**2·00**	0·525 510	−0·011 809
0·86	0·720 419	−0·002 386	**2·10**	0·513 701	−0·011 229
0·87	0·718 033	−0·002 370	**2·20**	0·502 472	−0·010 690
0·88	0·715 663	−0·002 355	**2·30**	0·491 782	−0·010 191
0·89	0·713 308	−0·002 339	**2·40**	0·481 591	−0·009 726
0·90	0·710 969	−0·002 322	**2·50**	0·471 865	−0·009 292
0·91	0·708 647	−0·002 308	**2·60**	0·462 573	−0·008 887
0·92	0·706 339	−0·002 292	**2·70**	0·453 686	−0·008 509
0·93	0·704 047	−0·002 277	**2·80**	0·445 177	−0·008 154
0·94	0·701 770	−0·002 261	**2·90**	0·437 023	−0·007 824

Fig. 2.2. A table to determine the value of K [5]

2.3 Analytical Modeling of Inductors

Because of the increasing competition in the electronic industry, manufacturers need to produce better and better products and need to provide results to the customers about the working of their components. A useful solution to these problems, towards the recognition of the interior behavior of the components and the presentation of the working of them to the customers, is the modeling [10, 13, 14].

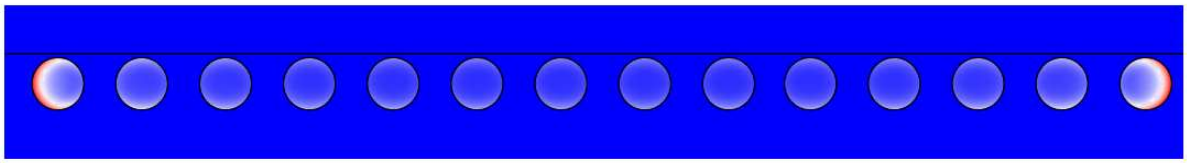

Fig. 2.3. The proximity effect in a coil

Of the three basic passive components, inductor is the most difficult one to model, because it is the most complex. We can highlight two specific parts of its complexity: the core and the conducting path. The conducting path is usually made of copper, either in wire form or as a thin layer of metal. By the reason of the skin effect at radio frequency, the resistance of this path will increase with the square root of frequency [10]. For isolated copper conductors, the skin depth at various frequencies is simple to calculate, with the following formula:

$$\delta = \frac{1}{\sqrt{\pi f \mu \sigma}}, \tag{2.16}$$

where δ the distance where the amplitude of the current flowing in a plane decreases by a factor e^{-1}. Because of the proximity effect, the skin depth becomes more complicated when turns in a winding are close to each other [12]. The core loss is another matter [10]. In the case of inductors with air core, ceramic or other nonmagnetic core, there is no, or minimal core loss. On the other hand, for iron or ferrite cores, the loss will be at least proportional to frequency [10].

In the recent past, engineers constructed several models to describe and to simulate the working of inductors. With the given knowledge, nowadays both of the parameters of inductors, such as impedance, inductance, quality factor and skin effect can be simulated by a sort of model.

In the paper *RF-inductor modeling for the 21st century* [10], Leslie Green shows a new implemented theoretical model, which can predict more correctly the behavior of an inductor at high frequencies, too. The starting point of his study is the well-known three-element model, which can be seen in Fig. 2.1. In the case of this model L represents the DC value of the inductance, and the capacitance can be calculated by the following expression,

$$C = \frac{1}{\omega^2 L}, \tag{2.17}$$

which comes from the Thomson's formula (2.8). The resistance in the model is not the DC resistance of the inductor but, rather, some different value that more accurately simulates the component around the operating frequency. Green points out that, this model predicts correctly the characteristics of the inductance and the impedance in a wide range of the frequency, however it does not correctly predict the position of the peak of Q. Towards the exact modeling, two more parameter resistances were added to the basic model. By this model it is possible to set the peak value and the peak position of the quality factor. With the new mathematical model the attributes of an inductor can be modeled correctly [10]. The impedance of the model can be calculated by the

following expression [10]:

$$\mathrm{Z} = \frac{1}{\frac{1}{R_S(\frac{f}{SRF})^{\eta}+\mathrm{j}2\pi fL} + \frac{1}{R_{HF}+\frac{1}{\mathrm{j}2\pi fC}}}, \tag{2.18}$$

where R_S is the series loss resistance, η is a parameter between 0.5 and 1 and R_{HF} modifies the frequency position of the maximum Q point. The determination of L and C happens in the same way than in the case of the old three element model. The quality factor can be calculated by the (2.11). The measured and the predicted quality factor after the setting of the parameters of the model can be seen in Fig. 2.4. The

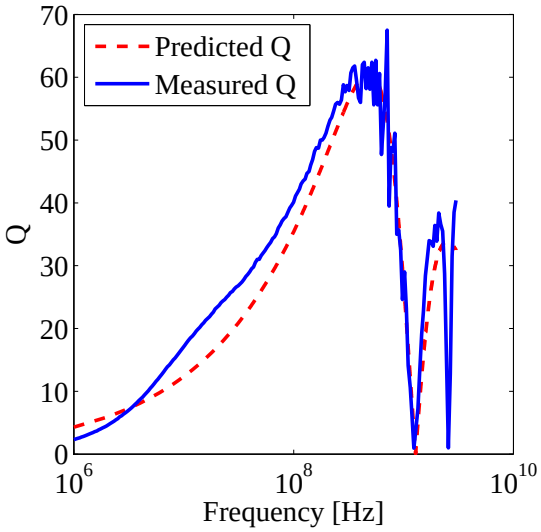

Fig. 2.4. The measured and the predicted quality factor by Green's model

setting the attributes of the examined inductor resulted the following values of the model components: $L = 180$ nH, $C = 85$ fF, $R_{HF} = 15\ \Omega$, $\eta = 0.54$, $R_S = 6.5\ \mathrm{m}\Omega$, $SRF = 1030$ MHz.

The results of presented works in the past two sections have been used to understand the internal working of inductors including the variation of the inductance, the impedance, the quality factor as a function of the frequency; and to check the correctness of the constructed finite element models, which will be shown below, in the next session.

2.4 The Finite Element Method

Sometimes it is necessary to solve more complex problems than, which can be difficult to work out in analytical way, such as the inductance of a nonlinear solenoid or the capacitance between two conductors with any kind of shape. In many cases, there are complex geometries in which difficult partial differential equations have to be solved. For example, the calculation the effect of the eddy current losses and the hysteresis losses in a power inductor having drum shaped core made of soft magnetic ferrit, is not an easy task analytically. The solving of this problem will be shown in chapter 4.

The finite element method (FEM) is a numerical technique for finding approximate solutions of partial differential equations (PDE). The steps of the buliding up of a finite

element simulation can be seen in Fig. 2.5 [15, 16, 18, 20–22]. The first step of a finite element simulation is the specification phase, when the geometry model of the real life problem have to plan in a CAD environment. Then the partial differential equation system and the boundary conditions have to be found out, which describe the working of the examined phenomena.

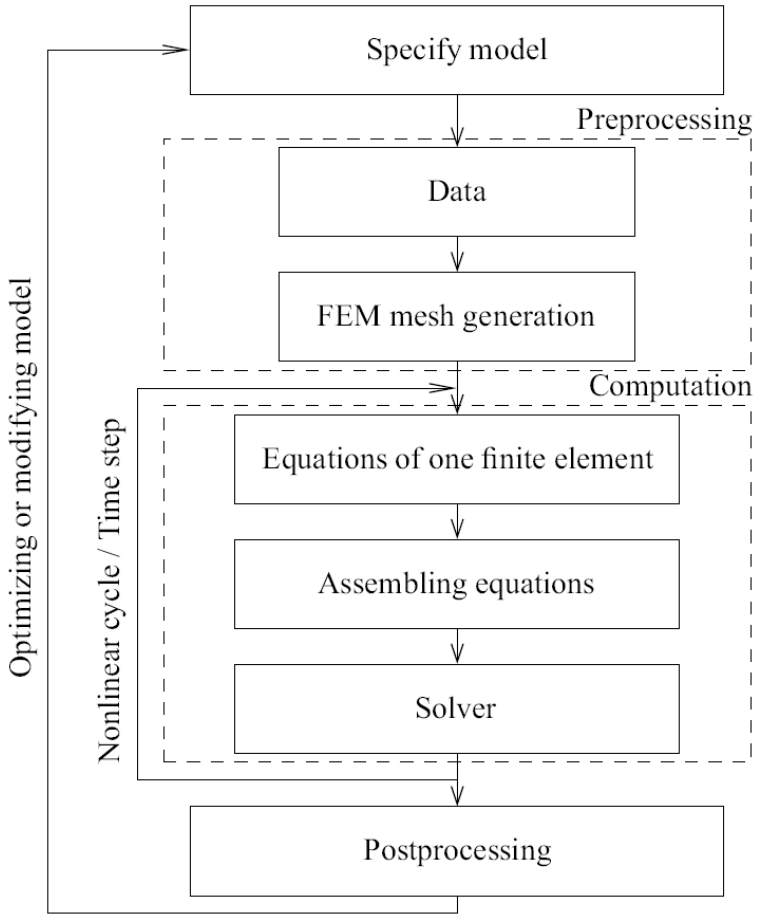

Fig. 2.5. The steps of simulation by FEM

The next step is the preprocessing task. Here the values of different parameters, such as the material properties, i.e. the constitutive relations, the excitation signal and the others have to be specified. The geometry can be simplified according to symmetries or axial symmetries.

The finite element method, as its name shows, based on the solution of finite numbers of units, which assembly leads to the result of the total problem. To divide the geometry into smaller elements, the geometry must be discretized by a FEM mesh [15, 21]. A finite element can be triangle or quadrangle in 2D, which can be seen in Fig. 2.6, and tetrahedron or hexahedron in 3D, which can be seen in Fig. 2.7. The triangle element has 3 nodes and 3 edges, the quadrangle element has 4 nodes and 4 edges. A tetrahedral element has 4 vertices and 6 edges and a hexahedral element has 8 nodes and 12 edges [15, 21]. In the case of nodal elements, the unknown potentials have to be solved at the vertices of the finite elements, but the potentials can be solved at the edges of the elements when we are using vector finite elements [].

There are some important rules, how to generate a mesh [15]. Neither overlapping

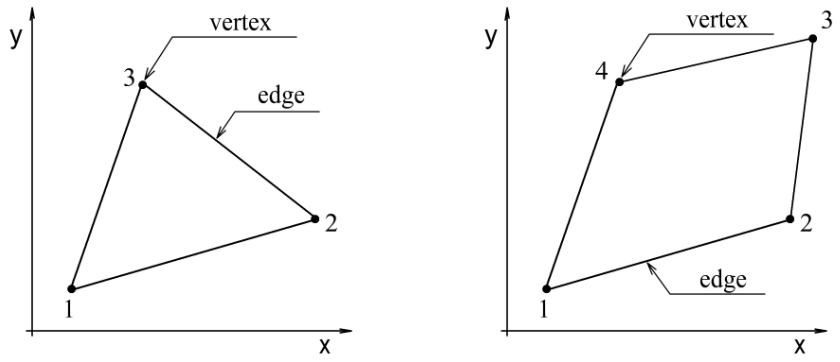

Fig. 2.6. 2D finite elements

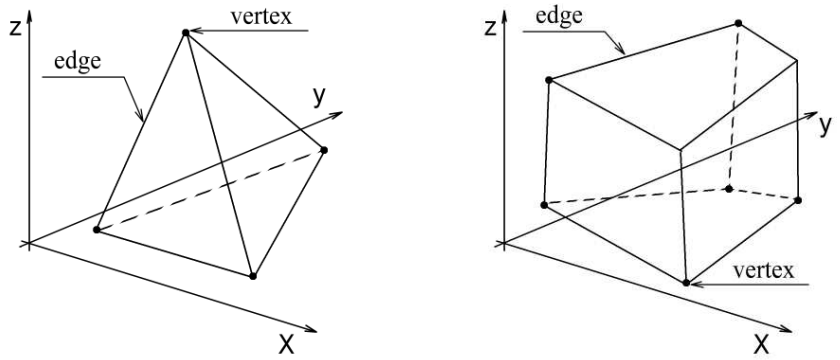

Fig. 2.7. 3D finite elements

nor holes are allowed in the generated finite element mesh. A two dimensional and a three dimensional FEM mesh can be seen in Fig. 2.8 and in Fig. 2.9 generated by the COMSOL Multiphysics software package [24]. The first one shows the 2D mesh of an SMT (Surface Mount Technology) inductor divided by triangular elements. The 3D FEM mesh shows a shielded version of an SMT power inductor divided by thetraedral finite elements; the mesh in air is not shown here.

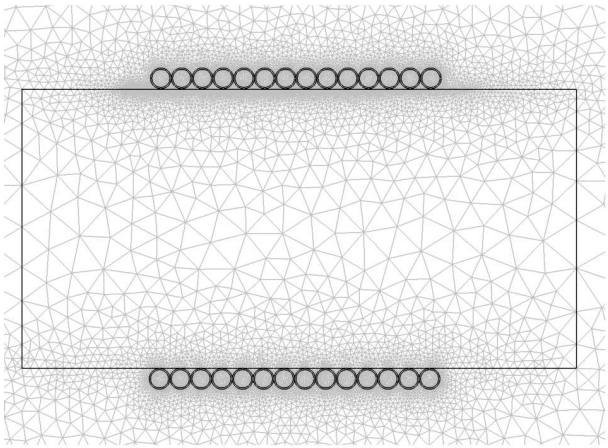

Fig. 2.8. 2D mesh of an inductor

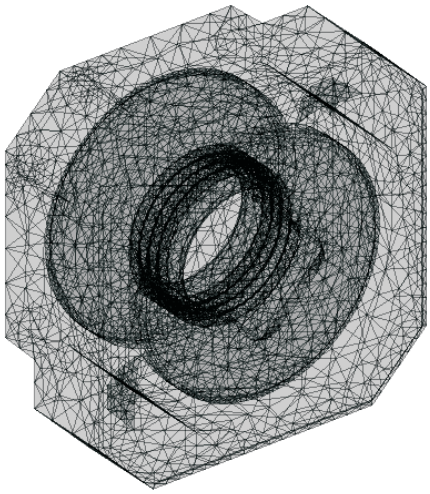

Fig. 2.9. 3D mesh of a power SMT inductor

The next step after discretizing of the geometry is solving the problem. The equations of the FEM model are based on the weak form of the potential formulation, which can be deduced from the basis equations, i.e. from the Maxwell's equations in the electrical engineering practice [15]. The equations must be set up on the level of one finite element. Assembling of these equations through the FEM mesh means the setting up of the global equation system of the problem, which solution leads to the approximation of the introduced potential. The equation system of the examined phenomena can be linear or nonlinear, depending on the medium to be analyzed. After the setting up of this global system of equations, it must be solved by a solver. If the constitutive equations are nonlinear the computation may contain iteration, for example in the case when the simulation of ferromagnetic materials with nonlinear characteristics must be executed. Iteration means that the system of equations must be set up and must be solved step by step until convergence is reached. The solution must be worked out at every discrete time step if the problem is time dependent [16].

The outcome of the computations provides the approximation of the potential values in the vertices or in the edges of the FEM mesh. Any electromagnetic field quantity, such as magnetic field intensity, magnetic flux density, etc. or various attributes, such as inductance, capacitance, energy, force can be calculated by using potentials. In the postprocessing stage there is a chance to modify the geometry, the material parameters or the FEM mesh to get more accurate results. In Fig. 2.10 a 2D result of an SMT inductor can be seen at radio frequency. The surface plot and the arrows represent the magnetic flux density inside the component, which is modified by the skin- and the proximity effects. The magnetic flux density is also shown inside the open and the shielded version of an SMT power inductor in Fig. 2.11.

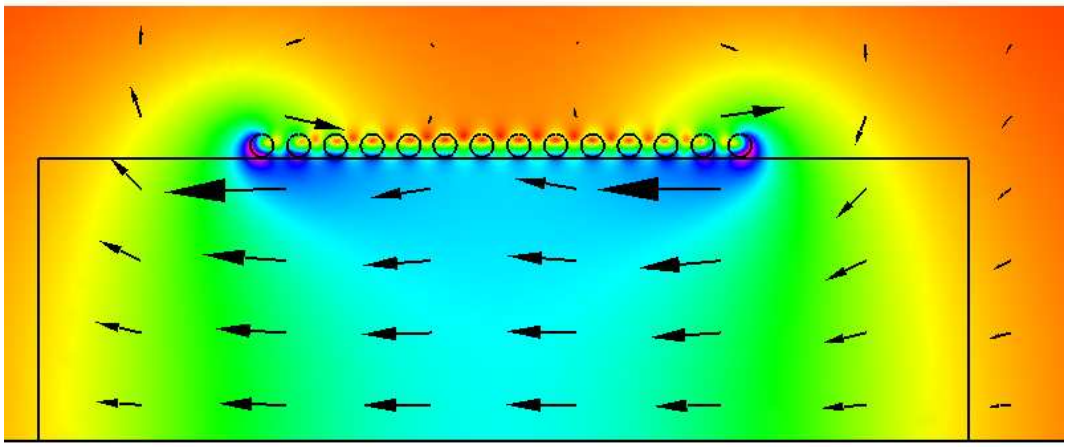

Fig. 2.10. Magnetic flux density inside an SMT inductor

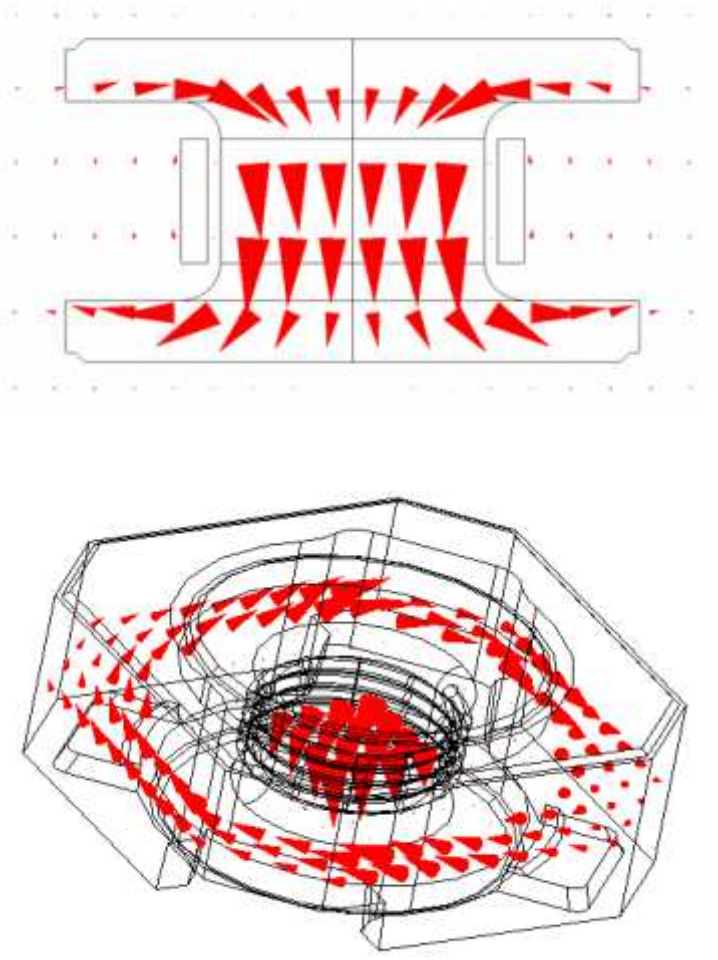

Fig. 2.11. Magnetic flux density inside an SMT power inductor

Chapter 3

Theoretical Background

3.1 The Maxwell's Equations

3.1.1 The integral form and the differential form

Every electromagnetic phenomena can be characterized by a partial differential equation system, which also known as Maxwell's equations [25]. This equation system defines relationship between electromagnetic field quantities, such as electric field intensity $\boldsymbol{E}$, magnetic field intensity $\boldsymbol{H}$, electric flux density $\boldsymbol{D}$, magnetic flux density $\boldsymbol{B}$ and the source densities, such as electric current density $\boldsymbol{J}$ and the electric charge density ρ.

The numerical analysis or the computer aided design (CAD) of an arrangement, which requires electromagnetic field calculation can be executed according to the Maxwell's equations, which are the following [25]:

$$\oint_l \boldsymbol{H} \cdot \mathrm{d}\boldsymbol{l} = \int_\Gamma \left(\boldsymbol{J} + \frac{\partial \boldsymbol{D}}{\partial t} \right) \cdot \mathrm{d}\boldsymbol{\Gamma}, \tag{3.1}$$

$$\oint_l \boldsymbol{E} \cdot \mathrm{d}\boldsymbol{l} = - \int_\Gamma \frac{\partial \boldsymbol{B}}{\partial t} \cdot \mathrm{d}\boldsymbol{\Gamma}, \tag{3.2}$$

$$\oint_\Gamma \boldsymbol{B} \cdot \mathrm{d}\boldsymbol{\Gamma} = 0, \tag{3.3}$$

$$\oint_\Gamma \boldsymbol{D} \cdot \mathrm{d}\boldsymbol{\Gamma} = \int_\Omega \rho \, \mathrm{d}\Gamma. \tag{3.4}$$

However, the above equation system, which known as the integral form of Maxwell's equations, is expressive and it is the classical form of the them. When building up of potential formulations of electromagnetic field problems, it is easier to use the differential form of this collection of equations. The differential form of the Maxwell's equations are the following [20]:

$$\nabla \times \boldsymbol{H} = \boldsymbol{J} + \frac{\partial \boldsymbol{D}}{\partial t}, \tag{3.5}$$

$$\nabla \times \boldsymbol{E} = - \frac{\partial \boldsymbol{B}}{\partial t}, \tag{3.6}$$

$$\nabla \cdot \boldsymbol{B} = 0, \tag{3.7}$$

$$\nabla \cdot \boldsymbol{D} = \rho. \tag{3.8}$$

The first Maxwell's equation (3.1) or (3.5) is commonly called Ampere's law. This equation represents that the current density $\boldsymbol{J}$, which means the current flowing in coils – the summation of the source current density and the eddy currents inside a conducting material – and the displacement currents $\frac{\partial \boldsymbol{D}}{\partial t}$, which is generated by a time-varying electric field, generate a magnetic field intensity $\boldsymbol{H}$. The classical form of it says that the line integral of the magnetic field intensity vector along any closed loop l is equal to the summation of currents, which are determined by the surface integral of current densities flowing across the area Γ bounded by the line l. Fig. 3.1 shows a visualization of the Ampere's law.

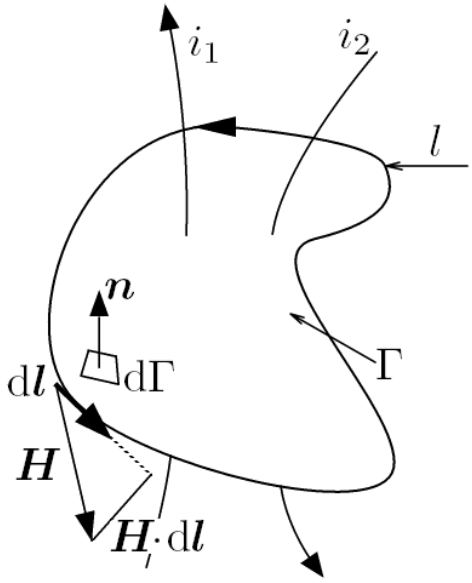

Fig. 3.1. Ampere's law

The second equation (3.2) or (3.6) is named Faraday's law. This equation describes that the time-varying magnetic field generates electric field. In time-dependent case the electric and the magnetic fields, i.e the first and the second Maxwell's equations are coupled. The time variation of the magnetic field effects electric field with reverse orientation in the studied region, and then the generated electric field generates eddy current inside the conducting material, which modifies the source magnetic fields. The integral form of the equation shows that the line integral of the electric field intensity vector along any closed loop l is equal to the surface integral of the time variation of the magnetic flux density vector across the area Γ bounded by the line l, as it can be seen in Fig. 3.2.

The third Maxwell's equation (3.3) or (3.7) is called the magnetic Gauss' law, which represents that the magnetic field is divergence-free. In other words the magnetic flux lines close upon themselves. The classical form shows that the surface integral of the magnetic flux density vector is equal to zero on a closed surface Γ, or in other words the flux lines are closed.

The electric Gauss' law (3.4) or (3.8) mean that the source of the electric field is the electric charge, moreover the electric flux lines start and close upon the charge. The integral form of the electric Gauss' law says that the surface integral of the electric flux density on a closed surface is equal to the volume integral of the charge density, and Γ

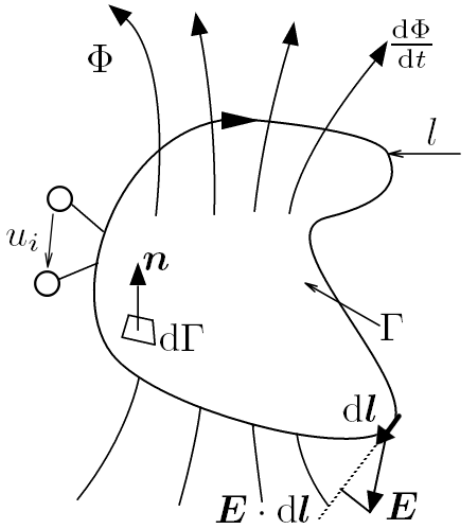

Fig. 3.2. Faraday's law

bounds Ω.

The macroscopic properties, i.e the characteristics of the examined materials can be defined by the so-called constitutive relations [15, 16, 25]:

$$\boldsymbol{B} = \mu_0(\boldsymbol{H} + \boldsymbol{M}), \tag{3.9}$$

$$\boldsymbol{D} = \varepsilon_0\varepsilon_r\boldsymbol{E} + \boldsymbol{P}, \tag{3.10}$$

$$\boldsymbol{J} = \sigma(\boldsymbol{E} + \boldsymbol{E_i}), \tag{3.11}$$

where $\boldsymbol{M}$ is the magnetization, $\boldsymbol{P}$ is the polarization, $\boldsymbol{E_i}$ is the impressed electric field, μ_0 is the permeability of vacuum, ε_0 is the permittivity of vacuum, ε_r is the relative permittivity and σ is the conductivity of the studied material. In air ϵ_r is equal to one, in magnetically linear material $\boldsymbol{M}$ is equal to zero, and $\boldsymbol{B} = \mu_0\mu_r\boldsymbol{H}$. In electrically linear material $\boldsymbol{P}$ is equal to zero.

3.1.2 The classification of Maxwell's equations

The Maxwell's equations can be classified to several forms [15]. In my thesis, three different potential formulations have been used, which are listed here.

In the simplest case the time variation of the source current is neglected, so the time independent current density $\boldsymbol{J_0}$ via the direct excitation current generates time independent magnetic field intensity $\boldsymbol{H}$ and magnetic flux density $\boldsymbol{B}$. The equations are the following:

$$\nabla \times \boldsymbol{H} = \boldsymbol{J_0}, \tag{3.12}$$

$$\nabla \cdot \boldsymbol{B} = 0, \tag{3.13}$$

and the constitutive relations. Taking the divergence of (3.12), the solenoidal property of the source current density can be got, i.e.

$$\nabla \cdot \boldsymbol{J_0} = 0. \tag{3.14}$$

The electric and the magnetic fields are coupled in time-varying case. The time dependent current density generates a time dependent magnetic field, which generates

electric field in the vicinity of the medium. The generated electric field effects eddy current in the conducting material, which modifies the source magnetic field intensity. If $|\boldsymbol{J}| >> |\frac{\partial \boldsymbol{D}}{\partial t}|$ the displacement currents can be neglected. The equations of an eddy current field are the following:

$$\nabla \times \boldsymbol{H} = \boldsymbol{J}, \tag{3.15}$$

$$\nabla \times \boldsymbol{E} = -\frac{\partial \boldsymbol{B}}{\partial t}, \tag{3.16}$$

$$\nabla \cdot \boldsymbol{B} = 0, \tag{3.17}$$

$$\boldsymbol{J} = \sigma \boldsymbol{E}, \tag{3.18}$$

and the appropriate constitutive relations must be added. Taking the divergence of the equation (3.15), the solenoidal property of the eddy current density can be obtained, i.e.

$$\nabla \cdot \boldsymbol{J} = 0. \tag{3.19}$$

At high frequencies the effect of the displacement currents cannot be neglected. In these cases the full form of the Maxwell's equations must be used.

3.1.3 Interface and boundary conditions

It is important to note, that if there are two materials Ω_1 and Ω_2 in the studied region, which are different in permeability, permittivity and conductivity, then interface conditions must be fulfilled on the boundary Γ. Fig. 3.3 shows material attributes and electromagnetic field quantities in the different materials. The normal unit vector $\boldsymbol{n}$ is equal to the outer normal unit vector of the medium.

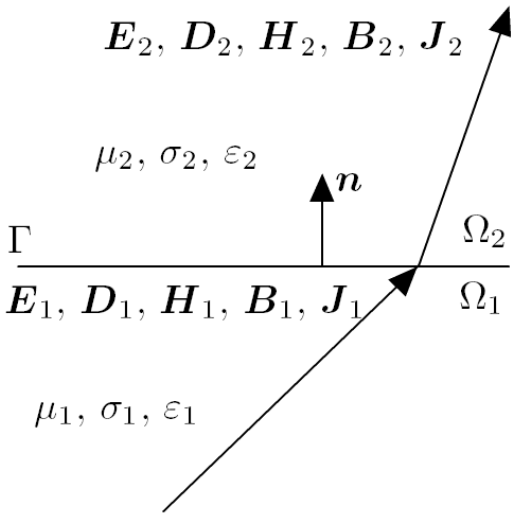

Fig. 3.3. Demonstration of the electromagnetic field quantities along an interface boundary

In the case of static magnetic field problems and in eddy current field problems the open boundary can be modeled by a sphere with a radius $r \to \infty$. The energy crossing the area of this boundary is equal to zero, because the variation of energy of electric and

magnetic field is taking place inside the bounding sphere. This condition can only be fulfilled if

$$\lim_{r\to\infty} r^2(\boldsymbol{E}\times\boldsymbol{H})\cdot\boldsymbol{n}=0, \tag{3.20}$$

i.e

$$\lim_{r\to\infty} r|\boldsymbol{E}|=0, \qquad \text{and} \qquad \lim_{r\to\infty} r|\boldsymbol{H}|=0. \tag{3.21}$$

This means that the electric and the magnetic fields must vanish at infinity.

In other words during the solution of Maxwell's equations, the interface and the boundary conditions must be considered along the interface of the materials and the boundary surfaces of the problem region.

Electric and magnetic field intensity

The interface conditions prescribe continuity for the tangential component of the electric field intensity,

$$\boldsymbol{n}\times(\boldsymbol{E_2}-\boldsymbol{E_1})=\boldsymbol{0}. \tag{3.22}$$

If there is no current density on the interface, the tangential component of the magnetic field intensity is continuous,

$$\boldsymbol{n}\times(\boldsymbol{H_2}-\boldsymbol{H_1})=\boldsymbol{0}. \tag{3.23}$$

If Γ denotes the bounding sphere of domain Ω_1, i.e. $\boldsymbol{E_2}=\boldsymbol{0}$ and $\boldsymbol{H_2}=\boldsymbol{0}$, moreover $\boldsymbol{E}=\boldsymbol{E_1}$ and $\boldsymbol{H}=\boldsymbol{H_1}$, then the boundary conditions can be written as

$$-\boldsymbol{n}\times\boldsymbol{E}=\boldsymbol{0}, \qquad \text{or} \qquad \boldsymbol{E}\times\boldsymbol{n}=\boldsymbol{0}, \tag{3.24}$$

and

$$-\boldsymbol{n}\times\boldsymbol{H}=\boldsymbol{0}, \qquad \text{or} \qquad \boldsymbol{H}\times\boldsymbol{n}=\boldsymbol{0}. \tag{3.25}$$

Electric and magnetic flux density

On the interface of different dielectric materials the normal component of the electric flux density is continuous only if there is no surface charge,

$$\boldsymbol{n}\cdot(\boldsymbol{D_2}-\boldsymbol{D_1})=0. \tag{3.26}$$

On the interface of different magnetic materials, the normal component of the magnetic flux density must be continuous,

$$\boldsymbol{n}\cdot(\boldsymbol{B_2}-\boldsymbol{B_1})=0. \tag{3.27}$$

The normal component of the conducting current must be continuous in the case of eddy current field,

$$\boldsymbol{n}\cdot(\boldsymbol{J_2}-\boldsymbol{J_1})=0, \tag{3.28}$$

or generally

$$\boldsymbol{n}\cdot(\boldsymbol{J_2}-\boldsymbol{J_1}+\boldsymbol{n}\cdot\left(\frac{\partial\boldsymbol{D_2}}{\partial t}-\frac{\partial\boldsymbol{D_1}}{\partial t}\right)=0, \tag{3.29}$$

is valid on the interface.

If Γ denotes the bounding sphere of domain Ω_1, i.e. $\boldsymbol{D_2} = \mathbf{0}$, $\boldsymbol{B_2} = \mathbf{0}$, $\boldsymbol{J_2} = \mathbf{0}$ and $\partial \boldsymbol{D_2}/\partial t = \mathbf{0}$, moreover $\boldsymbol{D} = \boldsymbol{D_1}$, $\boldsymbol{B} = \boldsymbol{B_1}$ and $\boldsymbol{J} = \boldsymbol{J_1}$ then the boundary conditions can be formulated as

$$-\boldsymbol{n} \cdot \boldsymbol{D} = 0, \qquad \text{or} \qquad \boldsymbol{D} \cdot \boldsymbol{n} = 0, \tag{3.30}$$

and

$$-\boldsymbol{n} \cdot \boldsymbol{B} = 0, \qquad \text{or} \qquad \boldsymbol{B} \cdot \boldsymbol{n} = 0, \tag{3.31}$$

and

$$-\boldsymbol{n} \cdot \boldsymbol{J} = 0, \qquad \text{or} \qquad \boldsymbol{J} \cdot \boldsymbol{n} = 0, \tag{3.32}$$

or generally,

$$-\boldsymbol{n} \cdot \boldsymbol{J} - \boldsymbol{n} \cdot \frac{\partial \boldsymbol{D}}{\partial t} = 0, \qquad \text{or} \qquad \boldsymbol{J} \cdot \boldsymbol{n} + \frac{\partial \boldsymbol{D}}{\partial t} \cdot \boldsymbol{n} = 0. \tag{3.33}$$

Absorbing boundary condition

In some cases, particulary at high frequencies it is important that the electromagnetic waves should not reflect from the artificial far boundary. Here, the so-called absorbing boundary condition can be used, which can be written as

$$\frac{1}{\mu_{r2}} \boldsymbol{n} \times (\nabla \times \boldsymbol{E}) - \frac{\mathrm{j}k_0}{\eta} \boldsymbol{n} \times (\boldsymbol{n} \times \boldsymbol{E}) = \mathbf{0}, \tag{3.34}$$

or

$$\frac{1}{\varepsilon_{r2}} \boldsymbol{n} \times (\nabla \times \boldsymbol{H}) - \mathrm{j}k_0 \eta \boldsymbol{n} \times (\boldsymbol{n} \times \boldsymbol{H}) = \mathbf{0}, \tag{3.35}$$

where $\eta = \sqrt{\mu_{r1}/\varepsilon_{r1}}$ is the normalized intrinsic impedance of medium 1, which equal to one in air, $k_0 = \omega\sqrt{\varepsilon_0 \mu_0}$, $\varepsilon_{r2} = 1$ and $\mu_{r2} = 1$. Substituting η, k_0 and μ_{r2} into (3.34) results in

$$\boldsymbol{n} \times (\nabla \times \boldsymbol{E}) - \mathrm{j}\omega\sqrt{\varepsilon_0 \mu_0} \cdot \boldsymbol{n} \times (\boldsymbol{n} \times \boldsymbol{E}) = \mathbf{0}, \tag{3.36}$$

where $\nabla \times \boldsymbol{E} = -j\omega\mu_0 \boldsymbol{H}$. After simplification, the absorbing boundary condition can be written as

$$\sqrt{\frac{\mu_0}{\varepsilon_0}} \boldsymbol{n} \times \boldsymbol{H} + \boldsymbol{n} \times (\boldsymbol{n} \times \boldsymbol{E}) = \mathbf{0}. \tag{3.37}$$

It is important to note that the above boundary condition can only be used in the case of sinusoidal excitation.

3.2 Potential Formulations

To solve an electromagnetic field problem, the partial differential equation system of the studied phenomenon must be simplified to a potential formulation. In the case of the presented static field, eddy current field and wave propagation field problem, three different potential formulations have been used. This section shows the determination of these potential formulations.

3.2.1 Static magnetic field

In static case, the basis equations are (3.12) and(3.13) and the linearized constitutive relations. First of all, the magnetic vector potential $\boldsymbol{A}$ must be defined as [15, 17, 18]

$$\boldsymbol{B} = \nabla \times \boldsymbol{A}, \tag{3.38}$$

which satisfies the magnetic Gauss' law (3.13), because of the mathematical identity $\nabla \cdot \nabla \times \boldsymbol{A} \equiv 0$. Substituting this equation into the first Maxwell's equation (3.12) and using the linear constitutive equation $\boldsymbol{H} = \nu \boldsymbol{B}$, the next partial differential equation can be got [15, 17, 18]:

$$\nabla \times (\nu \nabla \times \boldsymbol{A}) = \boldsymbol{J_0}, \text{ in } \Omega_0 \cup \Omega_m, \tag{3.39}$$

where ν is the reluctance, where $\nu = \frac{1}{\mu}$. The structure of a static magnetic field problem can be seen in Fig. 3.4, where Γ_B is the artificial far boundary, Γ_H is the symmetry plane, Ω_0 is the air, Ω_m is the magnetic material and $\boldsymbol{J_0}$ is the current density.

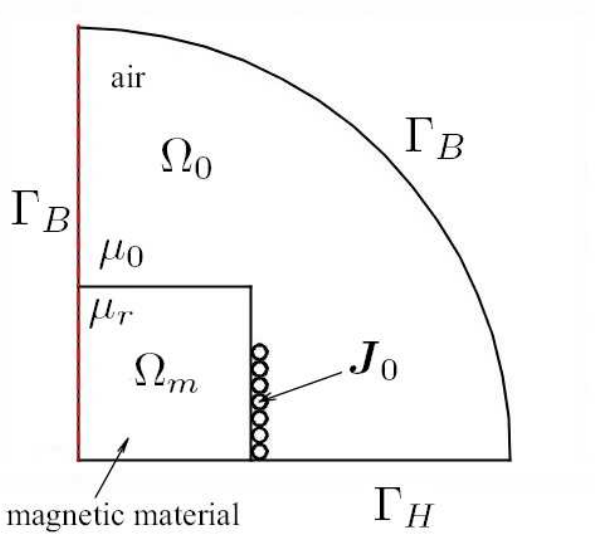

Fig. 3.4. Structure of a static magnetic field

Here it is important to note that if the static magnetic field problem is solved, the uniqueness of the magnetic vector potential must be ensured, which can be selected zero [15],

$$\nabla \cdot \boldsymbol{A} = 0, \tag{3.40}$$

which is usually called Coulomb gauge [15]. Substituting (3.40) into the equation of the static case and applying several mathematical transformations leads to the following equation, which is the gauged form of the $\boldsymbol{A}$-formulation [15].

$$\nabla \times (\nu \nabla \times \boldsymbol{A}) - \nabla(\nu \nabla \cdot \boldsymbol{A}) = \boldsymbol{J_0}, \text{ in } \Omega_0 \cup \Omega_m. \tag{3.41}$$

The deduction of the term $-\nabla(\nu \nabla \cdot \boldsymbol{A})$, which implies Coulomb gauge implicity is out of the scope of this work, it can be found in the literature [15]. Substituting the magnetic vector potential to the boundary condition (3.25) and by the reason of (3.31) leads to the following conditions [15]:

$$(\nu \nabla \times \boldsymbol{A}) \times \boldsymbol{n} = \boldsymbol{0}, \text{ on } \Gamma_H, \tag{3.42}$$

$$\boldsymbol{n} \times \boldsymbol{A} = \boldsymbol{0}, \text{ on } \Gamma_B. \tag{3.43}$$

The following boundary conditions can be determined according to the Coulomb gauge [15],

$$\boldsymbol{A} \cdot \boldsymbol{n} = 0, \text{ on } \Gamma_H, \tag{3.44}$$

$$\nu \nabla \cdot \boldsymbol{A} = 0, \text{ on } \Gamma_B. \tag{3.45}$$

The above equations can be used in the case of nodal elements.

If vector finite elements are used, first of all, the impressed current vector potential $\boldsymbol{T_0}$ must be defined [15]. Because the equation $\nabla \cdot \boldsymbol{J_0} = 0$ must be fulfilled, the rotation of the impressed current vector potential is equal to the current density, i.e.

$$\nabla \times \boldsymbol{T_0} = \boldsymbol{J_0}, \tag{3.46}$$

which term is important because of the consistency of the equation system. The following functional can be built up to determine the source term [15]:

$$\mathscr{F}\{\boldsymbol{T_0}\} = \int_\Omega |\nabla \times \boldsymbol{T_0} - \boldsymbol{J_0}|^2 \mathrm{d}\Omega_0 \cup \Omega_m, \tag{3.47}$$

which has to be minimized. The following equation is equivalent to the above one [15]:

$$\nabla \times \nabla \times \boldsymbol{T_0} = \nabla \times \boldsymbol{J_0}, \text{ in } \Omega_0 \cup \Omega_m, \tag{3.48}$$

and the boundary conditions are

$$\boldsymbol{T_0} \times \boldsymbol{n} = \boldsymbol{0}, \text{ on } \Gamma_H, \tag{3.49}$$

$$\boldsymbol{T_0} \cdot \boldsymbol{n} = 0, \text{ on } \Gamma_B. \tag{3.50}$$

Applying the above results the ungauged form of the $\boldsymbol{A}$-formulation can be got,

$$\nabla \times (\nu \nabla \times \boldsymbol{A}) = \nabla \times \boldsymbol{T_0}, \text{ in } \Omega_0 \cup \Omega_m, \tag{3.51}$$

$$(\nu \nabla \times \boldsymbol{A}) \times \boldsymbol{n} = \boldsymbol{0}, \text{ on } \Gamma_H, \tag{3.52}$$

$$\boldsymbol{n} \times \boldsymbol{A} = \boldsymbol{0}, \text{ on } \Gamma_B. \tag{3.53}$$

Here $\nabla \cdot \boldsymbol{A} = 0$ can be satisfied by the use of vector finite elements, which has the divergence-free property.

3.2.2 Eddy current field

Eddy current field is defined by the equations (3.15)-(3.18). To solve eddy current field problems the $\boldsymbol{A}$,V-formulation has been used with vector and nodal elements [19].

In the conducting region Ω_c, the magnetic vector potential $\boldsymbol{A}$ and the electric scalar potential V have been used, but only the magnetic vector potential $\boldsymbol{A}$ has been used is the nonconducting region Ω_n. Consequently, two equations are needed. In Fig. 3.5 the structure of an eddy current field problem can be seen, where Γ_{H_c} and Γ_E bound the conducting region and Γ_{H_n} and Γ_B bound the nonconducting region.

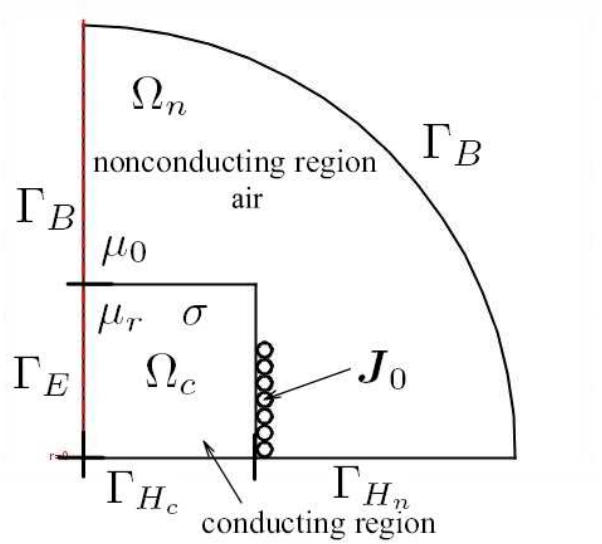

Fig. 3.5. Structure of an eddy current field

First of all, the electric scalar potential must be defined. Substituting (3.38) into Faraday's law (3.16) results the next expression:

$$\nabla \times \boldsymbol{E} = -\frac{\partial}{\partial t}\nabla \times \boldsymbol{A} = -\nabla \times \frac{\partial \boldsymbol{A}}{\partial t} \quad \Rightarrow \quad \nabla \times \left(\boldsymbol{E} + \frac{\partial \boldsymbol{A}}{\partial t}\right) = \boldsymbol{0}, \tag{3.54}$$

because derivation by space and derivation by time can be replaced. The term $\boldsymbol{E} + \frac{\partial \boldsymbol{A}}{\partial t}$ can be derived from the electric scalar potential V, because $\nabla \times \nabla v = \boldsymbol{0}$ for any scalar function v. The expression is the following:

$$\boldsymbol{E} + \frac{\partial \boldsymbol{A}}{\partial t} = -\nabla V, \tag{3.55}$$

finally, the electric field intensity can be determined by

$$\boldsymbol{E} = -\frac{\partial \boldsymbol{A}}{\partial t} - \nabla V. \tag{3.56}$$

Substituting (3.38) and (3.56) into (3.15) and using the linear form of the constitutive relations (3.9) and (3.18), lead to the first expression of the $\boldsymbol{A}$,V-formulation, which does not satisfy the Coulomb gauge. From the divergence-free property of the induced current density, the second relation can be deduced.

Here, the static magnetic and eddy current fields are coupled. The source current density of the coupled static magnetic field can be defined by the equation (3.51).

The equations and the boundary conditions of the ungauged $\boldsymbol{A}$,V-$\boldsymbol{A}$-formulation are the following [15]:

$$\nabla \times (\nu \nabla \times \boldsymbol{A}) + \sigma \frac{\partial \boldsymbol{A}}{\partial t} + \sigma \nabla V = \boldsymbol{0}, \text{ in } \Omega_c, \tag{3.57}$$

$$-\nabla \cdot \left(\sigma \frac{\partial \boldsymbol{A}}{\partial t} + \sigma \nabla V\right) = 0 \text{ in } \Omega_c, \tag{3.58}$$

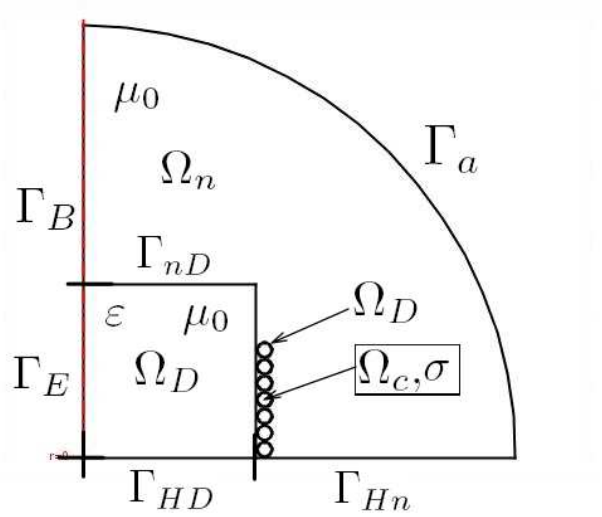

Fig. 3.6. Structure of a wave propagation problem

$$\nabla \times (\nu \nabla \times \boldsymbol{A}) = \nabla \times \boldsymbol{T_0}, \text{ in } \Omega_n, \tag{3.59}$$

$$(\nu_0 \nabla \times \boldsymbol{A}) \times \boldsymbol{n} = \boldsymbol{0}, \text{ on } \Gamma_{H_c}, \tag{3.60}$$

$$-\left(\sigma \frac{\partial \boldsymbol{A}}{\partial t} + \sigma \nabla V\right) \cdot \boldsymbol{n} = 0 \text{ on } \Gamma_{H_c}, \tag{3.61}$$

$$(\nu \nabla \times \boldsymbol{A}) \times \boldsymbol{n} = \boldsymbol{0}, \text{ on } \Gamma_{H_n}, \tag{3.62}$$

$$\boldsymbol{n} \times \boldsymbol{A} = \boldsymbol{0}, \text{ on } \Gamma_E, \tag{3.63}$$

$$V = V_0, \text{ on } \Gamma_E, \tag{3.64}$$

$$\boldsymbol{n} \times \boldsymbol{A} = \boldsymbol{0}, \text{ on } \Gamma_B, \tag{3.65}$$

$$\boldsymbol{n_c} \times \boldsymbol{A} + \boldsymbol{n_n} \times \boldsymbol{A} = \boldsymbol{0}, \text{ on } \Gamma_{nc}, \tag{3.66}$$

$$(\nu \nabla \times \boldsymbol{A}) \times \boldsymbol{n_c} + (\nu \nabla \times \boldsymbol{A}) \times \boldsymbol{n_n} = \boldsymbol{0}, \text{ on } \Gamma_{nc}, \tag{3.67}$$

$$-\left(\sigma \frac{\partial \boldsymbol{A}}{\partial t} + \sigma \nabla V\right) \cdot \boldsymbol{n} = 0, \text{ on } \Gamma_{nc}. \tag{3.68}$$

3.2.3 Wave propagation field

A wave propagation field can be computed quite similar to the eddy current field. Wave propagation problems were solved by the $\boldsymbol{A}$,V-$\boldsymbol{A}$ formulation, too, but the effect of the displacement currents to the equation system has been added. The equations of the wave propagation field problem is only shown in the case of sinusoidal excitation. The difference between eddy current field problems and wave propagation field problems is in the induced current density, which is the following:

$$\boldsymbol{J} = \sigma \boldsymbol{E} + \frac{\partial \boldsymbol{D}}{\partial t}. \tag{3.69}$$

In Fig. 3.6 the structure of a wave propagation field problem can be seen, where a dielectric material is bounded by Γ_E, Γ_{HD} and Γ_{nD}, and Γ_a is the artificial far boundary. Γ_{cD} is the boundary between the conducting material and the dielectric material. The equations are the following:

$$\nabla \times (\nu \nabla \times \boldsymbol{A}) - \omega^2 \varepsilon \boldsymbol{A} = \boldsymbol{0}, \text{ in } \Omega_n. \tag{3.70}$$

$$\nabla \times (\nu \nabla \times \boldsymbol{A}) + \mathrm{j}\omega\sigma \boldsymbol{A} = \boldsymbol{J_0}, \text{ in } \Omega_c. \tag{3.71}$$

$$\nabla \times (\nu \nabla \times \boldsymbol{A}) - \omega^2 \varepsilon \boldsymbol{A} = \boldsymbol{0}, \text{ in } \Omega_D. \tag{3.72}$$

$$\nu \nabla \times \boldsymbol{A} = \boldsymbol{0}, \text{ on } \Gamma_{H_n}, \tag{3.73}$$

$$\boldsymbol{n} \times \boldsymbol{A} = \boldsymbol{0}, \text{ on } \Gamma_B, \tag{3.74}$$

$$\boldsymbol{n_D} \times \boldsymbol{A} + \boldsymbol{n_n} \times \boldsymbol{A} = \boldsymbol{0}, \text{ on } \Gamma_{nD}, \tag{3.75}$$

$$(\nu \nabla \times \boldsymbol{A}) \times \boldsymbol{n_D} + (\nu \nabla \times \boldsymbol{A}) \times \boldsymbol{n_n} = \boldsymbol{0}, \text{ on } \Gamma_{nD}, \tag{3.76}$$

$$\boldsymbol{n_c} \times \boldsymbol{A} + \boldsymbol{n_D} \times \boldsymbol{A} = \boldsymbol{0}, \text{ on } \Gamma_{cD}, \tag{3.77}$$

$$(\nu \nabla \times \boldsymbol{A}) \times \boldsymbol{n_c} + (\nu \nabla \times \boldsymbol{A}) \times \boldsymbol{n_D} = \boldsymbol{0}, \text{ on } \Gamma_{cD}, \tag{3.78}$$

$$\boldsymbol{n} \times \boldsymbol{A} = \boldsymbol{0}, \text{ on } \Gamma_E, \tag{3.79}$$

$$\nu \nabla \times \boldsymbol{A} = \boldsymbol{0}, \text{ on } \Gamma_{H_D}, \tag{3.80}$$

$$(\nu \nabla \times \boldsymbol{A}) \times \boldsymbol{n_D} + (\nu \nabla \times \boldsymbol{A}) \times \boldsymbol{n_n} = \boldsymbol{0}, \text{ on } \Gamma_{nD}, \tag{3.81}$$

where (3.75) and (3.77) satisfy automatically. The absorbing boundary condition have been used on the artificial far boundary Γ_a. Substituting $\boldsymbol{H} = \nu_0 \nabla \times \boldsymbol{A}$ and $\boldsymbol{E} = -\mathrm{j}\omega \boldsymbol{A}$ into (3.37) results in

$$-\nu_0 \boldsymbol{n} \times \nabla \times \boldsymbol{A} + \mathrm{j}\omega \sqrt{\frac{\varepsilon_0}{\mu_0}} \boldsymbol{n} \times (\boldsymbol{n} \times \boldsymbol{A}) = \boldsymbol{0}, \text{ on } \Gamma_a. \tag{3.82}$$

3.3 The Weak Formulation

The finite element simulation is based on the solution of the weak form of the presented potential formulations [21–23]. The weak form of a partial differential equation can be obtained by using the weighted residual method [15]. This is a family of methods for solving partial differential equations. In this section the determination of the weak form of the above potential formulations will be presented.

The weak form of a potential formulation can be built up by using the partial differential equations and the boundary conditions of the example [15]. The potential function $\boldsymbol{A}$ is approximated by a function $\tilde{\boldsymbol{A}}$, i.e. $\boldsymbol{A} \cong \tilde{\boldsymbol{A}}$, moreover $\boldsymbol{T_0} \cong \tilde{\boldsymbol{T}}_{\boldsymbol{0}}$ and $V \cong \tilde{V}$. The weighted residual method is based on the inner product of the partial differential equation and a weighting function $\boldsymbol{W}$ [15].

3.3.1 Static magnetic field

The weak form of the $\boldsymbol{A}$-formulation, which satisfies the Coulomb gauge can be built up by using the equation (3.41) and the Neumann type boundary conditions (3.42) and (3.45). The equation is the following [15]:

$$\begin{aligned}\int_\Omega \boldsymbol{W_k}\cdot[\nabla\times(\nu\nabla\times\tilde{\boldsymbol{A}})-\nabla(\nu\nabla\cdot\tilde{\boldsymbol{A}})]\mathrm{d}\Omega+\int_{\Gamma_H}\boldsymbol{W_k}\cdot[(\nu\nabla\times\tilde{\boldsymbol{A}})\times\boldsymbol{n}]\mathrm{d}\Gamma\\ +\int_{\Gamma_B}\nu\nabla\cdot\tilde{\boldsymbol{A}}(\boldsymbol{W_k}\cdot\boldsymbol{n})\mathrm{d}\Gamma=\int_\Omega\boldsymbol{W_k}\cdot\boldsymbol{J_0}\,\mathrm{d}\Omega,\end{aligned}\tag{3.83}$$

where

$$\boldsymbol{n}\times\boldsymbol{W_k}=\boldsymbol{0},\ \text{on}\ \Gamma_B,\tag{3.84}$$

and

$$\boldsymbol{W_k}\cdot\boldsymbol{n}=0,\ \text{on}\ \Gamma_H,\tag{3.85}$$

moreover $k=1,\ldots,J$, where J is the element number of an entire function set $\boldsymbol{W_k}$. With the notation $\partial\Omega=\Gamma_H\cup\Gamma_B$, and by using the mathematical identity

$$\nabla\cdot(\varphi\boldsymbol{v})=\boldsymbol{v}\cdot\nabla\varphi+\varphi\nabla\cdot\boldsymbol{v},\tag{3.86}$$

and

$$\nabla\cdot(\boldsymbol{u}\times\boldsymbol{v})=\boldsymbol{v}\cdot\nabla\times\boldsymbol{u}-\boldsymbol{u}\cdot\nabla\times\boldsymbol{v},\tag{3.87}$$

where $\varphi=\nu\nabla\tilde{\boldsymbol{A}}$, $\boldsymbol{v}=\boldsymbol{W_k}$ and $\boldsymbol{u}=\nu\nabla\times\tilde{\boldsymbol{A}}$ the equation (3.83) can be reformulated to the following equation [15]:

$$\begin{aligned}&\int_\Omega[\nu(\nabla\times\boldsymbol{W_k})\cdot(\nabla\times\tilde{\boldsymbol{A}})+\nu\nabla\cdot\boldsymbol{W_k}\nabla\cdot\tilde{\boldsymbol{A}}]\mathrm{d}\Omega\\ &+\int_{\Gamma_H\cup\Gamma_B}[(\nu\nabla\times\tilde{\boldsymbol{A}})\times\boldsymbol{W_k}]\cdot\boldsymbol{n}\,\mathrm{d}\Gamma-\int_{\Gamma_H\cup\Gamma_B}\nu\nabla\cdot\tilde{\boldsymbol{A}}(\boldsymbol{W_k}\cdot\boldsymbol{n})\mathrm{d}\Gamma\\ &+\int_{\Gamma_H}\boldsymbol{W_k}\cdot[(\nu\nabla\times\tilde{\boldsymbol{A}})\times\boldsymbol{n}]\mathrm{d}\Gamma+\int_{\Gamma_B}\nu\nabla\cdot\tilde{\boldsymbol{A}}(\boldsymbol{W_k}\cdot\boldsymbol{n})\mathrm{d}\Gamma\\ &=\int_\Omega\boldsymbol{W_k}\cdot\boldsymbol{J_0}\,\mathrm{d}\Omega.\end{aligned}\tag{3.88}$$

The first and the third boundary integrals can be eliminated on Γ_H, because the first one can be written as

$$\begin{aligned}[(\nu\nabla\times\tilde{\boldsymbol{A}})\times\boldsymbol{W_k}]\cdot\boldsymbol{n}&=[\boldsymbol{n}\times(\nu\nabla\times\tilde{\boldsymbol{A}})]\cdot\boldsymbol{W_k}\\ &=-\boldsymbol{W_k}\cdot[(\nu\nabla\times\tilde{\boldsymbol{A}})\times\boldsymbol{n}].\end{aligned}\tag{3.89}$$

The rest part of the first boundary integral in Γ_B is equal to zero, because there the Dirichlet boundary condition(3.84) must be satisfied, and

$$[(\nu\nabla\times\tilde{\boldsymbol{A}})\times\boldsymbol{W_k}]\cdot\boldsymbol{n}=[\boldsymbol{W_k}\times\boldsymbol{n}]\cdot(\nu\nabla\times\tilde{\boldsymbol{A}})=-[\boldsymbol{n}\times\boldsymbol{W_k}]\cdot(\nu\nabla\times\tilde{\boldsymbol{A}}).\tag{3.90}$$

The second and the fourth boundary integrals are vanishing on Γ_B, moreover on Γ_H the Dirichlet boundary condition $\boldsymbol{W_k}\cdot\boldsymbol{n}=0$ must be used, so the second boundary integral

can be eliminated, too. Finally, the weak form of the $\boldsymbol{A}$-formulation, which satisfies the Coulomb gauge is the following [15]:

$$\int_\Omega [\nu(\nabla \times \boldsymbol{W_k}) \cdot (\nabla \times \boldsymbol{W_k}) + \nu \nabla \cdot \boldsymbol{W_k} \nabla \cdot \tilde{\boldsymbol{A}}] \mathrm{d}\Omega = \int_\Omega \boldsymbol{W_k} \cdot \boldsymbol{J_0} \, \mathrm{d}\Omega, \tag{3.91}$$

where $k = 1, \ldots, J$. This formulation have been used in the case of nodal finite elements.

Analogous by this way, the weak form of the ungauged $\boldsymbol{A}$-formulation can be described by using the equation (3.51) and the boundary condition (3.52) [15],

$$\int_\Omega \boldsymbol{W_k} \cdot [\nabla \times (\nu \nabla \times \tilde{\boldsymbol{A}})] \mathrm{d}\Omega + \int_{\Gamma_H} \boldsymbol{W_k} \cdot [(\nu \nabla \times \tilde{\boldsymbol{A}}) \times \boldsymbol{n}] \mathrm{d}\Gamma = \int_\Omega \boldsymbol{W_k} \cdot (\nabla \times \boldsymbol{T_0}) \mathrm{d}\Omega, \tag{3.92}$$

where $k = 1, \ldots, J$ and

$$\boldsymbol{n} \times \boldsymbol{W_k} = \boldsymbol{0}, \text{ on } \Gamma_B. \tag{3.93}$$

After the reformulations, the equation results in,

$$\begin{aligned} &\int_\Omega \nu(\nabla \times \boldsymbol{W_k}) \cdot (\nabla \times \tilde{\boldsymbol{A}}) \mathrm{d}\Omega \\ &+ \int_{\Gamma_H \cup \Gamma_B} [(\nu \nabla \times \tilde{\boldsymbol{A}}) \times \boldsymbol{W_k}] \cdot \boldsymbol{n} \mathrm{d}\Gamma + \int_{\Gamma_H} \boldsymbol{W_k} \cdot [(\nu \nabla \times \tilde{\boldsymbol{A}}) \times \boldsymbol{n}] \mathrm{d}\Gamma \\ &= \int_\Omega (\nabla \times \boldsymbol{W_k}) \cdot \tilde{\boldsymbol{T}}_\mathbf{0} \, \mathrm{d}\Omega + \int_{\Gamma_H \cup \Gamma_B} (\tilde{\boldsymbol{T}}_\mathbf{0} \times \boldsymbol{W_k}) \cdot \boldsymbol{n} \, \mathrm{d}\Gamma. \end{aligned} \tag{3.94}$$

The boundary integrals can be eliminated in the same way, which presented in relations (3.89) and (3.90). The boundary term on the right hand side can be eliminated, too, because it can be rewritten as

$$(\tilde{\boldsymbol{T}}_\mathbf{0} \times \boldsymbol{W_k}) \cdot \boldsymbol{n} = (\boldsymbol{W_k} \times \boldsymbol{n}) \cdot \tilde{\boldsymbol{T}}_\mathbf{0} = -(\boldsymbol{n} \times \boldsymbol{W_k}) \cdot \tilde{\boldsymbol{T}}_\mathbf{0}, \tag{3.95}$$

where the second term is zero on Γ_H according to (3.49) and the last one is zero on Γ_B according to (3.50). Consequently, the weak form of the ungauged $\boldsymbol{A}$-formulation is [15]

$$\int_\Omega [\nu(\nabla \times \boldsymbol{W_k}) \cdot (\nabla \times \boldsymbol{W_k})] \mathrm{d}\Omega = \int_\Omega (\nabla \times \boldsymbol{W_k}) \cdot \boldsymbol{T_0} \, \mathrm{d}\Omega. \tag{3.96}$$

where $k = 1, \ldots, J$. This formulation have been used in the case of vector finite elements.

3.3.2 Eddy current field

The weak formulation of the ungauged $\boldsymbol{A}$,V-$\boldsymbol{A}$-formulation can be got from the equations (3.57), (3.59) and the boundary conditions (3.60), (3.62) and (3.67). The electric scalar potential V should be replaced by the function v defined by

$$v(t) = \int_{-\infty}^{t} V(\tau) \mathrm{d}\tau, \tag{3.97}$$

from which

$$V(t) = \frac{\partial v(t)}{\partial t}. \tag{3.98}$$

Function v can be approximated by $\tilde{v}$, i.e. $v \cong \tilde{v}$. In the case of coupled static and eddy current fields, the impressed current vector potential has the property that

$$\nabla \times \boldsymbol{T_0} = \begin{cases} \boldsymbol{J_0}, & \text{in } \Omega_n, \\ \boldsymbol{0}, & \text{in } \Omega_c. \end{cases} \tag{3.99}$$

The first form of the weak formulation is the following [15]:

$$\begin{aligned} &\int_{\Omega_c} \boldsymbol{W_k} \cdot [\nabla \times (\nu \nabla \times \tilde{\boldsymbol{A}})] \mathrm{d}\Omega + \int_{\Omega_c} \boldsymbol{W_k} \cdot \left(\sigma \frac{\partial \tilde{\boldsymbol{A}}}{\partial t} + \sigma \nabla \frac{\partial \tilde{v}}{\partial t} \right) \mathrm{d}\Omega \\ &+ \int_{\Omega_n} \boldsymbol{W_k} \cdot [\nabla \times (\nu \nabla \times \tilde{\boldsymbol{A}})] \mathrm{d}\Omega + \int_{\Gamma_{H_c} \cup \Gamma_{H_n}} \boldsymbol{W_k} \cdot [(\nu \nabla \times \tilde{\boldsymbol{A}}) \times \boldsymbol{n}] \mathrm{d}\Gamma \\ &+ \int_{\Gamma_{nc}} \boldsymbol{W_k} \cdot [(\nu \nabla \times \tilde{\boldsymbol{A}}) \times \boldsymbol{n_c} + (\nu \nabla \times \tilde{\boldsymbol{A}}) \times \boldsymbol{n_n}] \mathrm{d}\Gamma \\ &= \int_{\Omega_c \cup \Omega_n} \boldsymbol{W_k} \cdot (\nabla \times \tilde{\boldsymbol{T}}_{\boldsymbol{0}}) \mathrm{d}\Omega, \end{aligned} \tag{3.100}$$

where $\boldsymbol{n} \times \boldsymbol{W_k} = \boldsymbol{0}$ on $\Gamma_E \cup \Gamma_B$, and $k = 1, \ldots, J$. The reformulation of this expression by using the identity $\nabla \cdot (\boldsymbol{u} \times \boldsymbol{u}) = \boldsymbol{v} \cdot \nabla \times \boldsymbol{u} - \boldsymbol{u} \cdot \nabla \times \boldsymbol{v}$, with the notation $\boldsymbol{v} = \boldsymbol{W_k}$ and $\boldsymbol{u} = \nu \nabla \times \tilde{\boldsymbol{A}}$, or on the right side $\boldsymbol{v} = \boldsymbol{W_k}$ and $\boldsymbol{u} = \tilde{\boldsymbol{T}}_{\boldsymbol{0}}$ and the simplification of the obtained expression leads to the first equation of the weak form of the ungauged $\boldsymbol{A}$,V-$\boldsymbol{A}$-formulation

$$\begin{aligned} &\int_{\Omega_c} \nu (\nabla \times \boldsymbol{W_k}) \cdot (\nabla \times \tilde{\boldsymbol{A}}) \mathrm{d}\Omega + \int_{\Omega_c} \boldsymbol{W_k} \cdot \left(\sigma \frac{\partial \tilde{\boldsymbol{A}}}{\partial t} + \sigma \nabla \frac{\partial \tilde{v}}{\partial t} \right) \mathrm{d}\Omega \\ &+ \int_{\Omega_n} \nu (\nabla \times \boldsymbol{W_k}) \cdot (\nabla \times \tilde{\boldsymbol{A}}) \mathrm{d}\Omega = \int_{\Omega_c \cup \Omega_n} (\nabla \times \boldsymbol{W_k}) \cdot \tilde{\boldsymbol{T}}_{\boldsymbol{0}} \mathrm{d}\Omega. \end{aligned} \tag{3.101}$$

The second equation can be got from the partial differential equation (3.58), with the boundary condition (3.61) and the interface condition (3.68). The conditions are multiplied by -1,

$$-\int_{\Omega_c} N_k \nabla \cdot \left(\sigma \frac{\partial \tilde{\boldsymbol{A}}}{\partial t} + \sigma \nabla \frac{\partial \tilde{v}}{\partial t} \right) \mathrm{d}\Omega + \int_{\Gamma_{H_c} \cup \Gamma_{nc}} N_k \left(\sigma \frac{\partial \tilde{\boldsymbol{A}}}{\partial t} + \sigma \nabla \frac{\partial \tilde{v}}{\partial t} \right) \cdot \boldsymbol{n} \mathrm{d}\Gamma = 0, \tag{3.102}$$

moreover $N_k = 0$ on Γ_E, and $k = 1, \ldots, I$, where N_k is a weighting function and I is the number of the nodes in the whole mesh. After mathematical reformulations the boundary integral terms are vanishing on Γ_{H_c} and Γ_{nc}. The second equation of the weak form of the ungauged $\boldsymbol{A}$,V-$\boldsymbol{A}$-formulation can be written as

$$\int_{\Omega_c} \nabla N_k \cdot \left(\sigma \frac{\partial \tilde{\boldsymbol{A}}}{\partial t} + \sigma \nabla \frac{\partial \tilde{v}}{\partial t} \right) \mathrm{d}\Omega = 0, \tag{3.103}$$

where $k = 1, \ldots, J$ and $k = 1, \ldots, I$.

3.3.3 Wave propagation field

Applying the weighted residual method to the partial differential equations (3.70), (3.71), (3.72) and the Neumann type boundary conditions (3.73), (3.76), (3.78) and (3.80)-(3.82 similar to the eddy current fields, leads to the weak form of the ungauged $\boldsymbol{A}$,V-$\boldsymbol{A}$-formulation in wave propagation case,

$$\begin{aligned}
&\int_{\Omega_n} \boldsymbol{W_k} \cdot [\nabla \times (\nu \nabla \times \tilde{\boldsymbol{A}}) - \omega^2 \varepsilon \tilde{\boldsymbol{A}}] \mathrm{d}\Omega + \int_{\Omega_c} \boldsymbol{W_k} \cdot [\nabla \times (\nu \nabla \times \tilde{\boldsymbol{A}}) + \mathrm{j}\omega\sigma \tilde{\boldsymbol{A}}] \mathrm{d}\Omega \\
&+ \int_{\Omega_D} \boldsymbol{W_k} \cdot [\nabla \times (\nu \nabla \times \tilde{\boldsymbol{A}}) - \omega^2 \varepsilon \tilde{\boldsymbol{A}}] \mathrm{d}\Omega + \int_{\Gamma_{Hn}} \boldsymbol{W_k} \cdot [(\nu \nabla \times \tilde{\boldsymbol{A}}) \times \boldsymbol{n}] \mathrm{d}\Gamma \\
&+ \int_{\Gamma_{nD}} \boldsymbol{W_k} \cdot [(\nu \nabla \times \tilde{\boldsymbol{A}}) \times \boldsymbol{n_D} + (\nu \nabla \times \tilde{\boldsymbol{A}}) \times \boldsymbol{n_n}] \mathrm{d}\Gamma \\
&+ \int_{\Gamma_{nD}} \boldsymbol{W_k} \cdot [(\nu \nabla \times \tilde{\boldsymbol{A}}) \times \boldsymbol{n_D} + (\nu \nabla \times \tilde{\boldsymbol{A}}) \times \boldsymbol{n_n}] \mathrm{d}\Gamma \\
&+ \int_{\Gamma_{cD}} \boldsymbol{W_k} \cdot [(\nu \nabla \times \tilde{\boldsymbol{A}}) \times \boldsymbol{n_c} + (\nu \nabla \times \tilde{\boldsymbol{A}}) \times \boldsymbol{n_D}] \mathrm{d}\Gamma + \int_{\Gamma_{HD}} \boldsymbol{W_k} \cdot [(\nu \nabla \times \tilde{\boldsymbol{A}}) \times \boldsymbol{n}] \mathrm{d}\Gamma \\
&+ \int_{\Gamma_a} \boldsymbol{W_k} \cdot [-\nu_0 \boldsymbol{n} \times \nabla \times \tilde{\boldsymbol{A}} + \mathrm{j}\omega \sqrt{\frac{\varepsilon_0}{\mu_0}} \boldsymbol{n} \times (\boldsymbol{n} \times \boldsymbol{A})] \mathrm{d}\Gamma = \boldsymbol{0}.
\end{aligned} \tag{3.104}$$

Using the mathematical identity $\nabla \cdot (\boldsymbol{u} \times \boldsymbol{v}) = \boldsymbol{v} \cdot \nabla \times \boldsymbol{u} - \boldsymbol{u} \cdot \nabla \times \boldsymbol{v}$ and the Gauss' theorem the equation can be reformulated as

$$\begin{aligned}
&\int_{\Omega_n \cup \Omega_D} \nu (\nabla \times \boldsymbol{W_k}) \cdot (\nabla \times \tilde{\boldsymbol{A}}) \mathrm{d}\Omega + \int_{\Gamma_{Hn} \cup \Gamma_a \cup \Gamma_B \cup \Gamma_{nD}} [(\nu \nabla \times \tilde{\boldsymbol{A}}) \times \boldsymbol{W_k}] \boldsymbol{n} \, \mathrm{d}\Gamma \\
&- \int_{\Omega_n \cup \Omega_D} \boldsymbol{W_k} \omega^2 \varepsilon \tilde{\boldsymbol{A}} \, \mathrm{d}\Omega + \int_{\Omega_c} \nu \nabla \times \boldsymbol{W_k} \nabla \times \tilde{\boldsymbol{A}} \, \mathrm{d}\Omega \\
&+ \int_{\Omega_c D} [(\nu \nabla \times \tilde{\boldsymbol{A}}) \times \boldsymbol{W_k}] \boldsymbol{n} \, \mathrm{d}\Gamma + \int_{\Omega_c} \boldsymbol{W_k} \mathrm{j}\omega\sigma \tilde{\boldsymbol{A}} \, \mathrm{d}\Omega \\
&+ \int_{\Gamma_E \cup \Gamma_{HD} \cup \Gamma_{nD} \cup \Gamma_{cD}} [(\nu \nabla \times \tilde{\boldsymbol{A}}) \times \boldsymbol{W_k}] \boldsymbol{n} \, \mathrm{d}\Gamma + \int_{\Gamma_{Hn}} \boldsymbol{W_k} \cdot [(\nu \nabla \times \tilde{\boldsymbol{A}}) \times \boldsymbol{n}] \mathrm{d}\Gamma \\
&+ \int_{\Gamma_{nD}} \boldsymbol{W_k} \cdot [(\nu \nabla \times \tilde{\boldsymbol{A}}) \times \boldsymbol{n_D} + (\nu \nabla \times \tilde{\boldsymbol{A}}) \times \boldsymbol{n_n}] \mathrm{d}\Gamma \\
&+ \int_{\Gamma_{nD}} \boldsymbol{W_k} \cdot [(\nu \nabla \times \tilde{\boldsymbol{A}}) \times \boldsymbol{n_D} + (\nu \nabla \times \tilde{\boldsymbol{A}}) \times \boldsymbol{n_n}] \mathrm{d}\Gamma \\
&+ \int_{\Gamma_{cD}} \boldsymbol{W_k} \cdot [(\nu \nabla \times \tilde{\boldsymbol{A}}) \times \boldsymbol{n_c} + (\nu \nabla \times \tilde{\boldsymbol{A}}) \times \boldsymbol{n_D}] \mathrm{d}\Gamma + \int_{\Gamma_{HD}} \boldsymbol{W_k} \cdot [(\nu \nabla \times \tilde{\boldsymbol{A}}) \times \boldsymbol{n}] \mathrm{d}\Gamma \\
&+ \int_{\Gamma_a} \boldsymbol{W_k} \cdot [-\nu_0 \boldsymbol{n} \times \nabla \times \tilde{\boldsymbol{A}} + \mathrm{j}\omega \sqrt{\frac{\varepsilon_0}{\mu_0}} \boldsymbol{n} \times (\boldsymbol{n} \times \boldsymbol{A})] \mathrm{d}\Gamma = \boldsymbol{0},
\end{aligned} \tag{3.105}$$

where all of the boundary integrals have its own pair, moreover $\boldsymbol{n} \times \boldsymbol{W} = 0$ on Γ_B and on Γ_E.

After mathematical simplifications the weak form of the ungauged $\boldsymbol{A}$,V-$\boldsymbol{A}$-formulation

can be got with the absorbing boundary condition in wave propagation case,

$$\begin{aligned}&\int_{\Omega_n\cup\Omega_D}[\nu(\nabla\times\boldsymbol{W_k})\cdot(\nabla\times\tilde{\boldsymbol{A}})-\omega^2\varepsilon\tilde{\boldsymbol{A}}]\mathrm{d}\Omega\\+&\int_{\Omega_c}[\nu(\nabla\times\boldsymbol{W_k})\cdot(\nabla\times\tilde{\boldsymbol{A}})+\mathrm{j}\omega\sigma\tilde{\boldsymbol{A}}\boldsymbol{W_k}]\mathrm{d}\Omega\\+&\int_{\Gamma_a}\mathrm{j}\omega\sqrt{\frac{\varepsilon_0}{\mu_0}}\boldsymbol{W_k}\tilde{\boldsymbol{A}}\,\mathrm{d}\Gamma=\boldsymbol{0}.\end{aligned}\tag{3.106}$$

where $k=1,\ldots,J$.

Chapter 4

Simulation of Inductors in COMSOL Multiphysics

4.1 Problem 1: Increasing the Quality factor

4.1.1 Overview of the problem

EPCOS AG develops, manufactures and markets electronic components, modules and systems, focusing on fast-growing leading-edge technology markets: in information technology (IT) and telecommunications, but also in automotive, industrial and consumer electronics. To satisfy the private demand of some customers EPCOS needs to design new components and modify the actual parameters of several types of inductors. The company has a developing team to find out the best geometry, material, and manufacturing process of inductors. Many researches are under way about improving the attributes of their components, such as the inductance, quality factor, maximum current, sensitivity and so on, through applying new materials and new geometries, which are also developing there [26].

One of the actual developments is the increasing of the quality factor of an RF SMT inductor. The reason of the work is that high quality factor is important in several cases, for example in oscillators, and because of that some of the customers want to use this inductor with super high quality factor (SHQ). The specification SHQ means in this case that the value of the quality factor must be at least 60 between 85 MHz and 110 MHz. In the present, this value is about 30 in this range as it can be seen in Fig. 4.1, which shows the actual quality factor as a function of the frequency. It seems that the achievable value of it is quite far from the present value, so the first step is to increase the quality factor if it is possible. This way is the modification of the winding without the modification of the geometry of the core and the used materials. The core of the inductor is a standard one, so it cannot be modified. Several winding type – closely- and widely spaced coils, and various diameters of winding wire – have been prepared, measured and simulated to found the best arrangement of the coils on the core.

The mentioned type of inductor is marked SIMID 0805-F, where 0805 means an international standard about the size of SMT (Surface Mount Technology) components not only inductors. Accordingly, the object of the project is an SMT inductor, which is usually working in the range of the radio frequency. The dimensions of the component are 1.24±0.04 mm × 1.22±0.04 mm × 2.03±0.04 mm. The component has a cubic coil on ferrite or ceramic core, depending on the aplication field of it. The winding wire is

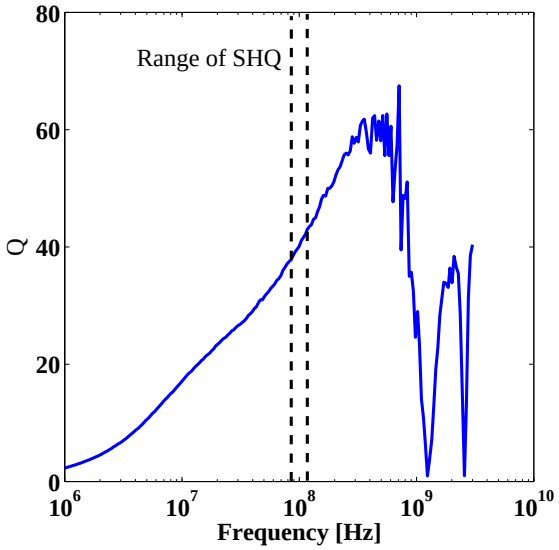

Fig. 4.1. Present value of Q

welded to the thick film coating on its terminations, which is made of silver, palladium and platinum or in an other case it is made of wolfram, nickel and gold. It has a flat top made of epoxy for vacuum pickup. The major features of the inductor are the high resonant frequency, which is between 300 MHz and 9 GHz depending on the type of the component and the close inductance tolerance. This type of inductor is used in resonant circuits, antenna amplifiers, mobile phones, Digital Enhanced Cordless Telecommunications (DECT) systems, car access systems, tire pressure monitoring systems (TPMS), wireless communication systems and global positioning systems (GPS). The microscopic photo of the component can be seen in Fig. 4.2.

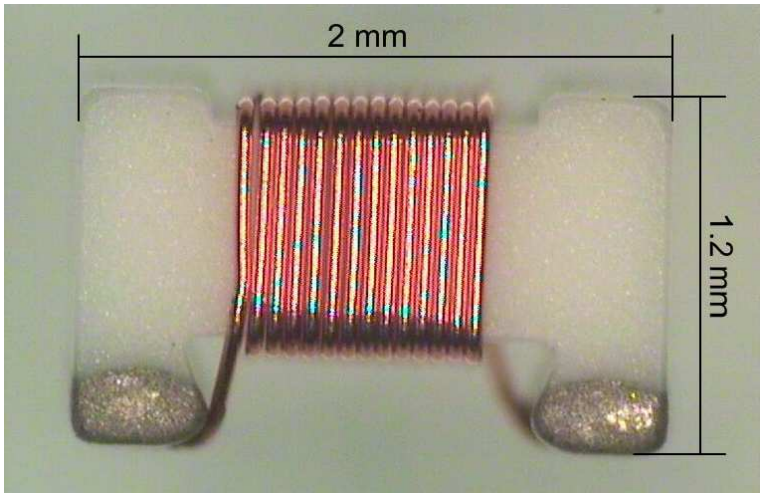

Fig. 4.2. The microscopic photo of the inductor

It is important to note that different applications need different values of inductance, resistance, maximum current and quality factor. The most of the parameters can be changed easily by the modification of the winding wire or the material of the core, but

the modification of one parameter causes variation in the other parameters as well. For example, if the inductance of the component is modified via the modification of the winding, i.e. the number of turns is increased or the distance between adjacent coils are decreased, the resistance of the inductor is increasing, the quality factor is decreasing and the SRF is also decreasing both in the two cases. But the reason of the variation of the attributes are different in the mentioned two examples. In the first case, the resistance is increasing in the effect of the more coils, because more coil means higher resistance, the quality factor is decreasing according to the expression of the quality factor, and the SRF is decreasing through the higher capacitance between the coils. In the second case, the resistance is increasing by the reason of the higher proximity effect between the coils, which get closer to each other, the Q-factor is decreasing because of the increasing of the resistance, finally, the SRF is decreasing through the high capacitance between the closer coils. It seems that it is not an easy task to improve parameters without the deterioration of other ones. In Fig. 4.3 and in Fig. 4.4, the family of this type of inductors can be seen, where the mentioned variations in the SRF, the resistance and the Q-factor are noticeable. It is important to note that between 2.7 nH and 820 nH inductors are manufactured with ceramic core and over 1 μH they are made with ferrite core. The reason of this is that the higher value of the inductance is only achievable with higher permeability of the core. However ferrite core has disadvantages, such as the eddy current losses and the hysteresis losses, so the quality factor of a ceramic core inductor can be higher.

The examined inductor was chosen from the 0805 family. Our plan is to improve one component, and in the possession of the results, the improvement can be extended to the whole family of this type of inductors. The chosen component is the one, which has 180 nH of inductance. It has 14 turns in one layer winding on a ceramic core. The used type of the ceramics named Rubalit 710, which is made of aluminum-oxide in 99.6 percent. The surface of the Rubalit 710 can be seen in Fig. 4.5. The relative permittivity ε_r of this material is 10. This type of ceramic designed to resist high mechanical, thermal and electrical loads and between this circumstances to provide long reliability. High strength and thermal conductivity are the characterizing features of these substrate materials. Ceramics are popular and well-tried materials in electronics, because of its minimal losses and low thermal conductivity, too, as it can be seen in Fig. 4.6. Fig. 4.7 shows the comparison of three ceramic made of aluminum-oxide. The coil of the examined inductor is made of enameled copper wire with 50 μm diameter. During the simulation the conductivity of the copper wire ($\sigma = 5.7 \cdot 10^7 \frac{\mathrm{S}}{\mathrm{m}}$) and the relative permittivity of the enamel insulation ($\varepsilon_r = 5$) of it are needed to consider.

4.1.2 The challenges

The research is divided into two parts. The first is the simulation way, where a finite element model was built up in the COMSOL Multiphysics software package [24,29,30] to simulate the interior working of an inductor, moreover to examine the winding geometries of the coil and to find out the best arrangement of it considering the quality factor and the nominal value of the inductance. The second way was the manufacturing and the measuring of the trial components, which was made in virtue of the finite element models. To check the correctness of the obtained numerical results experimental tests were executed.

L_R nH	Tolerance [1]	f_L MHz	Q_{min}	f_Q MHz	I_R mA	R_{max} Ω	$f_{res,min}$ MHz
Core material: ceramics							
2,7	± 10%	250	50	1500	1000	0.03	9000
5,6	≙ K	250	50	1000	900	0.04	7000
6,8		250	50	1000	800	0.05	6000
8,2		250	50	1000	700	0.09	5000
10	± 2%	250	50	500	700	0.09	5000
12	≙ G	250	50	500	700	0.09	4000
15	± 5%	250	50	500	650	1.13	3300
18	≙ J	250	60	500	700	0.08	3300
22		250	60	500	700	0.08	2500
27		250	60	500	700	0.09	2500
33		250	65	500	600	0.11	2200
39		250	65	500	600	0.12	2100
47		200	65	500	600	0.13	2000
56		200	60	500	600	0.14	1700
68		200	60	500	500	0.18	1600
82		150	60	500	500	0.19	1500
100		150	55	500	450	0.28	1350
120		150	50	250	440	0.31	1250
150		100	45	250	400	0.42	1150
180		100	45	250	340	0.53	1050
220		100	45	250	320	0.70	950
270		100	45	250	270	1.0	900
330		100	45	250	220	1.5	800
390		100	40	250	210	1.6	700
470		50	30	100	190	1.9	650
560		25	23	50	230	1.3	400
680		25	23	50	190	1.7	300

Fig. 4.3. Attributes of the 0805 family I [26]

L_R nH	Toler–ance [1)]	f_L MHz	Q_{min}	f_Q MHz	I_R mA	R_{max} Ω	$f_{res,min}$ MHz
Core material: ferrite							
1000	±5%	7.96	20	7.96	240	0.55	440
1200	≙ J	7.96	20	7.96	220	0.65	420
1500		7.96	20	7.96	200	0.70	380
1800		7.96	20	7.96	190	0.98	350
2200		7.96	20	7.96	130	1.60	330
2700		7.96	20	7.96	120	2.00	270
3300		7.96	20	7.96	100	3.30	250
3900		7.96	20	7.96	95	3.60	230
4700		7.96	20	7.96	90	3.80	210
5600		7.96	20	7.96	85	4.30	180
6800		7.96	20	7.96	80	4.70	140

Fig. 4.4. Attributes of the 0805 family II [26]

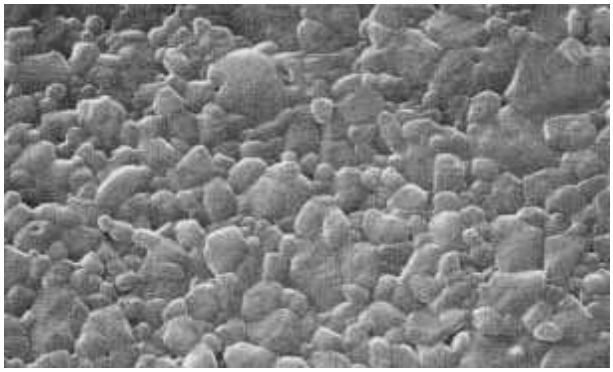

Fig. 4.5. The surface of Rubalit 710 [28]

The trial components were measured by an Agilent E4991A RF impedance and material analyzer which can be seen in Fig. 4.8. This type of analyzer provides a total solution for making easy, fast and accurate measurements of SMT devices and dielectric or magnetic materials from 1 MHz to 3 GHz. It has a user friendly Windows-style user interface and built in VBA (Visual Basic for Applications) programming function. It can communicate with other devices via LAN interface. It has several test fixtures to easily fix the small components or different materials to the instrument [27]. During the measurements of the trial components the Agilent 16197A SMD test fixture have been used which can be seen in Fig. 4.9. The manufacturing and the measuring of the trial components were made in the Hungarian part of EPCOS AG, Szombathely, Hungary.

To simulate the above problem, the COMSOL Multiphysics software package [24] have been used. The COMSOL Multiphysics is a finite element analysis and solver software package for various physics and engineering applications, especially coupled phenomena, or multiphysics. It also offers an extensive and well-managed interface to MATLAB [32] and its toolboxes for a large variety of programming, preprocessing and postprocessing possibilities. There is a similar built in interface, which is called COM-

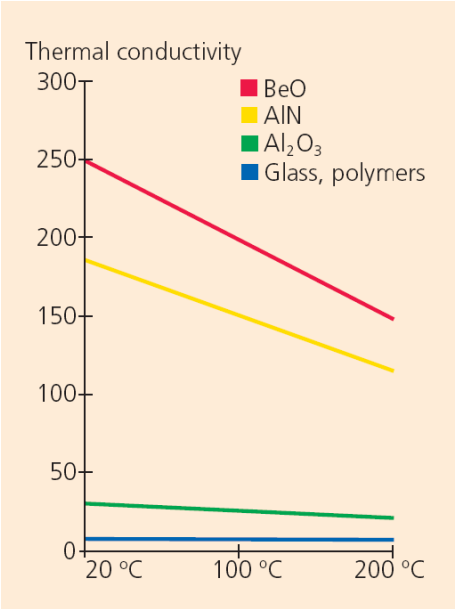

Fig. 4.6. The thermal conductivity of Al_2O_3 [28]

SOL Script [24]. The packages are running at several platforms, such as Windows, Mac/OS, Linux, Unix. In addition to the user-friendly simulation, which is based on the description of the physical phenomena, COMSOL Multiphysics also allows for entering coupled systems of partial differential equations (PDE). The PDE's can be entered directly or using the weak form. It has many modules, such as AC/DC Module, Acoustics Module, CAD Import Module, Chemical Engineering Module, Earth Science Module, Heat Transfer Module, Material Library, MEMS Module, RF Module and Structural Mechanics Module. The AC/DC Module is suitable to simulate electrical components and devices that depend on electrostatics, magnetostatics and electromagnetic quasi-statics applications, so this is the best part to simulate inductors, capacitors, motors and drives, and every electromagnetic phenomena.

The aim of the finite element simulation of the presented inductor and the examined problem is to built up a correct model to visualize the interior working of the component and predict the important attributes of it, such as the inductance, the impedance, the quality factor and the self-resonant frequency. The additional goal is to find out that it is possible to find a way to increase the quality factor through the modification of the winding, or not.

4.1.3 The two dimensional model

During the building up the model, the first problem was the complexity of the component. The largest problem was the cubical coil of the inductor, because in the COMSOL Multiphysics the flowing current in the coil can be described by a mathematical formula, which for example can be determined from the equation of the circle in the case of a helical coil.

That is the reason why the specialties of the core and the cubic coil were neglected and an axial symmetry model was created. In the engineering point of view the aims of a model are the efficiency, the speed and the simplicity, so the three dimensional

Property	Units	Rubalit® 708 S 96% Al_2O_3	Rubalit® 710 99.6% Al_2O_3	Alunit® AlN	Test per
Color	–	white	white	translucent medium gray	–
Medium grain size d_{50}	µm	3–5	2	4–5	–
Surface roughness R_a	µm	0.6 max	0.1	0.6 max	Profilometer (0.8 mm cutoff)
Bulk density	kg/m³	3780	3900	3330	ASTM C 20
Water absorption capacity	%	0	0	0	ASTM C 373
Bending strength - 4-point method (40 x 4 x 3 mm³) - dual-ring method (0.63 mm substrate thickness)	 MPa MPa	 400 500	 400	 360 	 ASTM F 417 DIN 52292
Modulus of elasticity	GPa	340	350	320	ASTM F 417
Thermal conductivity 20–100 °C	W/m °K	24	28	180	ASTM C 408
Specific heat	J/kg °K	800	800	738	
Coefficient of linear expansion 20 – 300 °C 20 – 600 °C 20 – 1000 °C	10^{-6}/°K	 6.8 7.3 8.0	 6.8 7.5 8.5	 4.7 5.2 5.6	ASTM C 372
Dielectric constant - 1 MHz - 1 GHz		 9.8 ± 10% 10.0 ± 10%	 10.1 ± 10% 10.1 ± 10%	 9.0 ± 10%	ASTM C 150
Dielectric loss factor (1 MHz)	10^{-3}	0.3	0.2	0.4	ASTM D 150
Breakdown voltage - 1 mm substrate thickness - 0.63 mm substrate thickness - 0.25 mm substrate thickness	KV/mm	 15 20 28	 >10 	 16 	ASTM D 149
Volume resistivity - 20 °C - 200 °C - 400 °C - 600 °C	Ohm x cm	 10^{13} 10^{12} 10^{11} 10^{8}	 10^{13} 10^{13} 10^{12} 10^{9}	 10^{13} 	ASTM D 257

Fig. 4.7. Indexes and parameters for ceramic substrates [28]

axial symmetry model was simplified to a two dimensional axial symmetry model. The COMSOL Multiphysics can handle 2D axial symmetry models, that is why this two models are equivalent. The procedure of the simplification can be seen in Fig. 4.10. During the 2D simulation two models were implemented. In the first case the excitation was a known voltage and in the second case excitation current was applied.

Fig. 4.8. Agilent E4991A RF impedance and material analyzer

Fig. 4.9. Agilent 16197A SMD Test Fixture

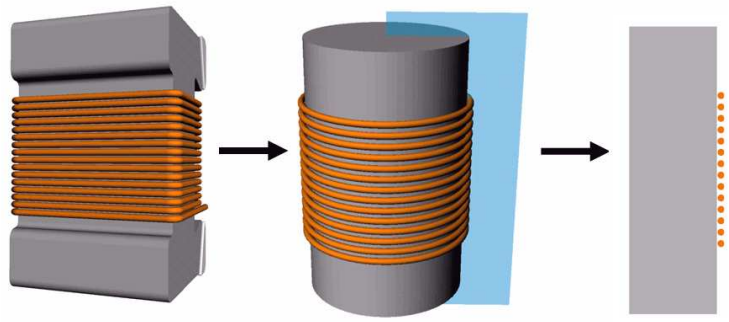

Fig. 4.10. The procedure of the simplification

4.1.4 The two dimensional simulation

Drawing the problem

The first step in the simulation is the drawing of the problem. COMSOL has a CAD part, which contains the basic drawing procedures, such as drawing dot, line, curve,

circle, rectangle, mirroring, scaling, chamfering, creating union and subsection, revolving, extruding, and so on [24]. It is quite good solution for creating two dimensional models, but sometimes it is not enough in the case of more difficult three dimensional problems. In these situations the CAD import module can be used, with which the models made with other CAD softwares, for example AutoCAD, Solid Works, etc. can be imported to the COMSOL Multiphysics.

To draw the above two dimensional model, first of all in the *New model* window the *2D axial symmetry* space dimension must be chosen. Then, as the core of the inductor a rectangle can be created with the corners 0 ; $1.015{\cdot}10^{-3}$ m, $6.2{\cdot}10^{-4}$ m; $-1.015{\cdot}10^{-3}$ m. The next step is drawing the coil. The diameter of the winding wire is 50 μm, and it has an enamel insulation. The average thickness of the wire with the insulation is 57.5 μm. So, the 14 turns can be drawn from 14 circles with the center coordinate $6.4875{\cdot}10^{-4}$, because the end of the ledge of the core is at $6.2{\cdot}10^{-4}$ m plus $57.5/2 \cdot 10^{-6}$ m, where the value of the coordinate means the distance from the axial symmetry axis. The insulation can be drawn from circles with the same center points, but the diameter of them are 57.5 μm. At last making the difference between the coil and the drawn circle is needed. The distance between the turns is the same as the manufactured inductor, it is 30 μm. The last step is the drawing of the bounding area, which is filled with air in this case. Let us draw a circle with the center point 0 ; 0 m, and cut half part of it. The drawn geometry can be seen in Fig. 4.11.

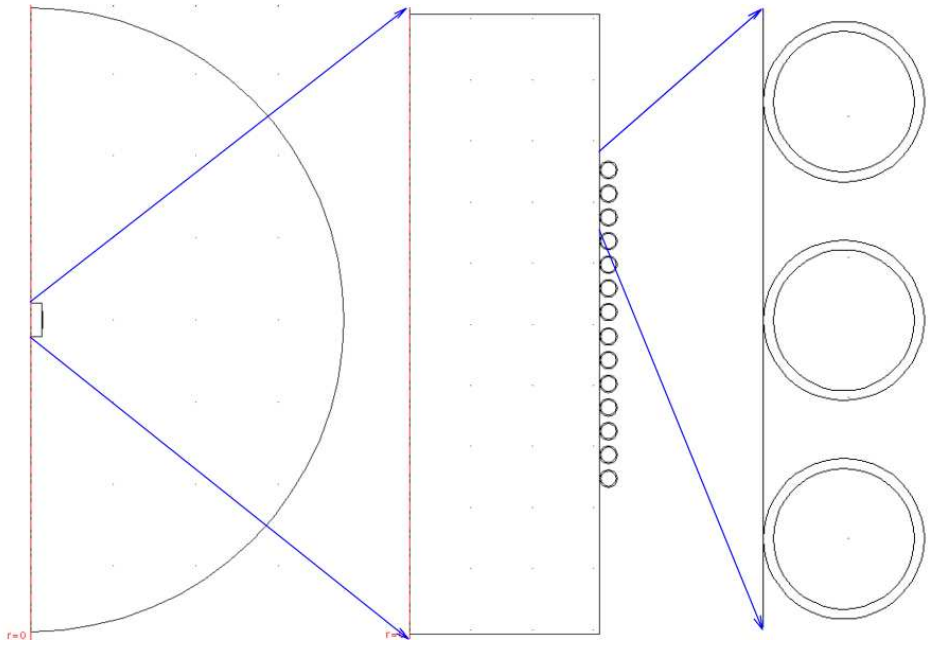

Fig. 4.11. The two dimensional geometry of the inductor in COMSOL Multiphysics

Preprocessing

The next task is the preprocessing, where the constants and some expressions must be set up. The constants can be set up at the *Options/Constants....* menu Here, the number of turns N, the conductivity σ marked *sigma*, the resistivity ϱ of the copper wire marked *ro*, the radius of the coil $r0$, the radius of the wire *rc*, the cross section of the wire A, the DC resistance of the model analytically *Rdc*, the parameter value of the capacitance C

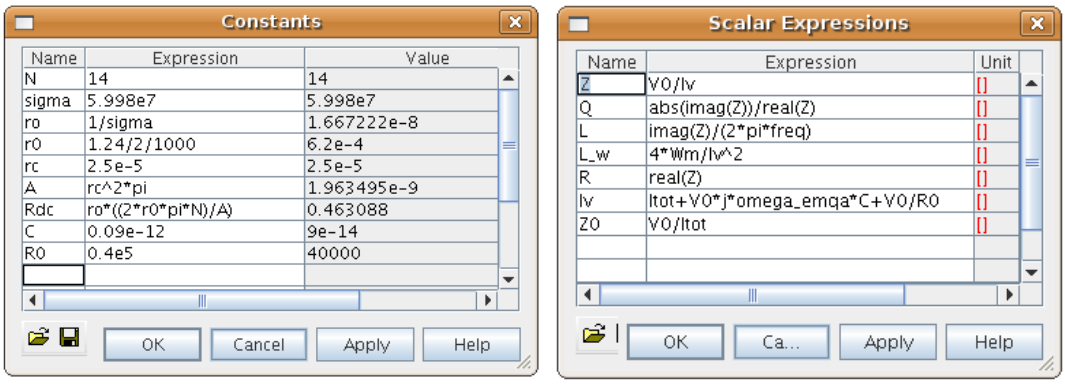

Fig. 4.12. The constants of and the scalar expressions of the model

and the resistance $R0$, are entered. The necessity of C and $R0$ will be shown later Fig. 4.12 shows the constants panel with the above constants.

The excitation voltage or the excitation current can be set up in the menu *Options/Expressions/Global Expressions...*, the value of the voltage is 1 V, and the value of the current is 1 A.

In the *Options/Integration Coupling Variables/Subdomain Variables...* menu the expressions can be set, which contain integrals. For example, during the simulation several quantities can be got from the impedance, i.e. the ratio of the excitation voltage across the inductor to the current through the component. In the first case of the 2D simulation, when the excitation is voltage, the current through the coil must be calculated by using the following integral in the surface of the coil Γ_{coil}:

$$I_{tot} = \int_{\Gamma_{coil}} J_\varphi \, \mathrm{d}\Gamma, \tag{4.1}$$

where J_φ is the φ-oriented total current density, which is equal to the sum of the potential current, which is generated by the potential different between the ends of the coil, the eddy currents and the displacement currents.

In the other case, when the current is known, the voltage across the component must be calculated, which can be done by using the following formula [30]:

$$V_0 = 2\pi r \frac{\int_{\Gamma_{coil}} (-\boldsymbol{E_\varphi} + \boldsymbol{J_\varphi}/\sigma) \mathrm{d}\Gamma}{S}, \tag{4.2}$$

where $\boldsymbol{E_\varphi}$ is the φ-oriented electric field intensity, σ is the conductivity of the wire and S is the cross section of the winding wire.

At the *Options/Expressions/Scalar Expressions...* the needed scalar expressions can be set up, which are in this case the expression of the impedance Z, the quality factor Q, the inductance from the impedance L and from the magnetic energy L_w, the resistance R, the modified total current density Iv, and the impedance of the model $Z0$ only. $omega_emqa$ is the angular frequency of the excitation and Wm is the magnetic energy. The necessity of Iv and $Z0$ will be shown later. The used scalar expressions of the model can be seen in Fig. 4.12, too.

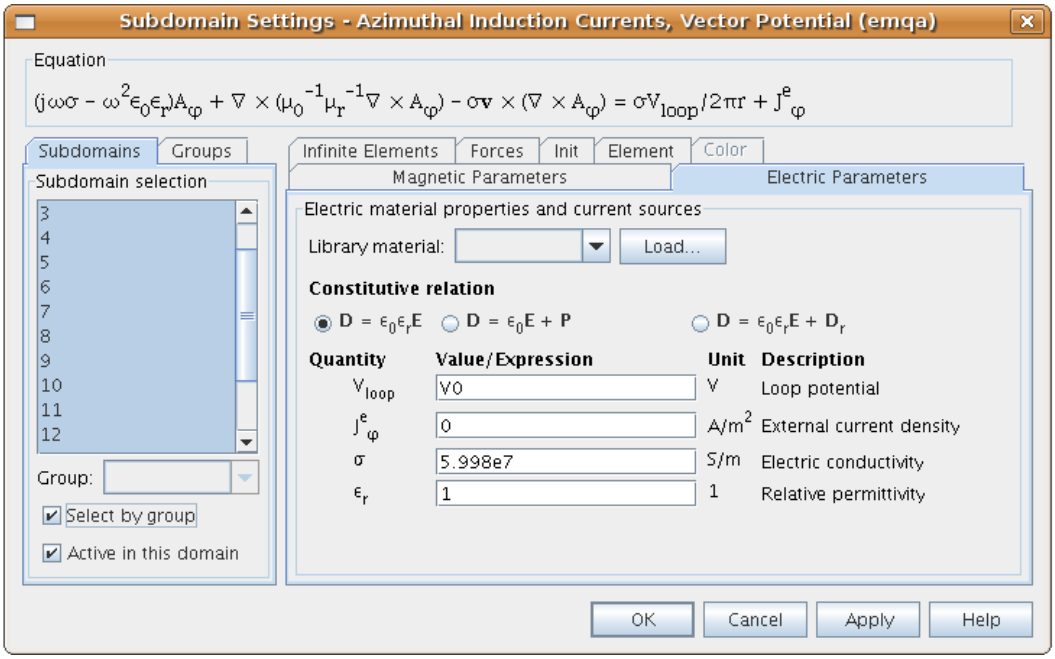

Fig. 4.13. The setting up of the material properties

Physics

To simulate a physical phenomenon the equations, which describe the studied problem must be known. In COMSOL Multiphysics there are three different ways to determine the needed equations. The first one is the entering of the weak form of the potential formulation, the second one is typing the partial differential equations. The last one is the using of the COMSOL built-in formulations. During the 2D simulation the built-in *Azimuthal Induction Currents, Vector Potential* formulation has been used, which can be deduced from the equations (3.70)-(3.72), with the notation that in 2D the electric scalar potential V is equal to zero [15] and the impressed current vector potential must not be used. Moreover it is important to note that the potential current can be determined by

$$\boldsymbol{J_p} = \sigma \frac{V_{loop}}{2\pi r}, \tag{4.3}$$

where V_{loop} is the voltage across a closed loop, σ is the conductivity of the wire, and r is the mean radius of the coil. Considering this facts and substituting $\mathrm{j}\omega$ instead of $\frac{\partial}{\partial t}$ and adding the definition of the potential current to the equation, lead to the following expression:

$$(\mathrm{j}\omega\sigma + \omega^2\varepsilon)\boldsymbol{A} + \nabla \times (\nu \nabla \times \boldsymbol{A}) = \boldsymbol{J_0} + \sigma \frac{V_{loop}}{2\pi r}. \tag{4.4}$$

After the determination of the equation system at the *Physics/Subdomain Settings...* menu the physical properties of the materials, such as the relative permeability, the relative permittivity and the conductivity, moreover the form of the constitutive relations and the excitation voltage or current can be set up as it can be seen in Fig. 4.13.

Then the boundary conditions must be set up at the *Physics/Boundary Settings...* menu. In this example two boundary conditions have been used. The first one $r = 0$ is applied on the axial symmetry axis. The second one is applied on the artificial far

boundary, i.e. the ledge of the air, which is represented by the outer circle. Here the so-called impedance boundary condition has been used, which can be described by [20,24,30]

$$\sqrt{\frac{\mu}{\varepsilon - j\sigma\omega}}\boldsymbol{n} \times \boldsymbol{H} + \boldsymbol{E}_{\boldsymbol{\varphi}} = -\boldsymbol{E}_{\boldsymbol{s\varphi}}, \tag{4.5}$$

where in this case $\boldsymbol{E}_{\boldsymbol{s\varphi}} = \boldsymbol{0}$, because there is no surface electric field, and $\sigma = 0$, because the conductivity of the air is equal to zero. Considering this notations the form of the equation (3.37) can be got, which is the so-called absorbing boundary condition. The setting panel of the boundary conditions can be seen in Fig. 4.14.

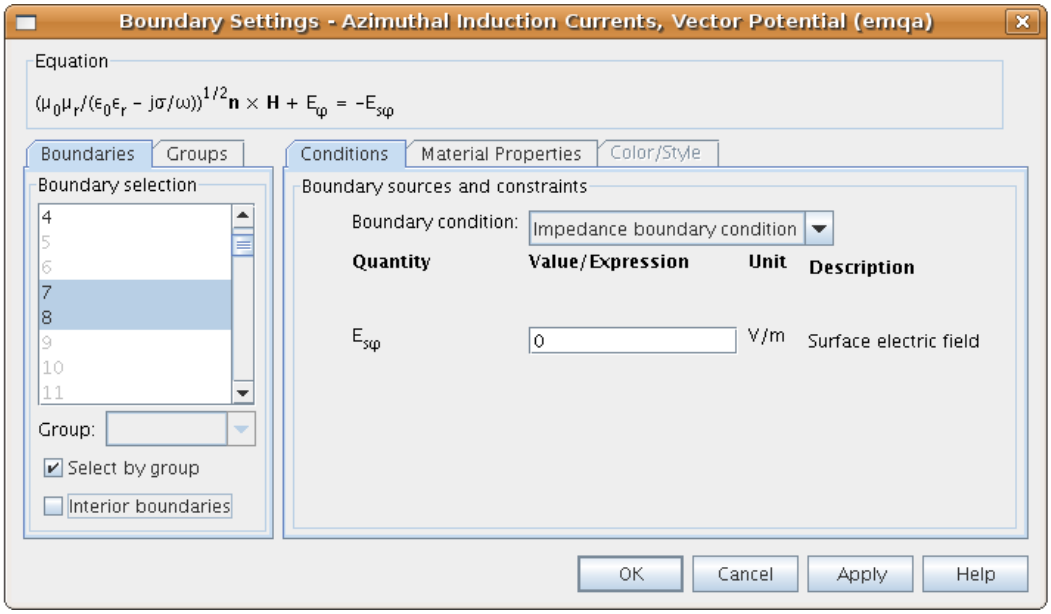

Fig. 4.14. Setting up of the boundary conditions

Meshing and solving the problem

The next step of the simulation procedure is the meshing, where the geometry of the problem is divided into finite elements. In COMSOL Multiphysics the mesh generator has many settings from the shape of the elements to the sizes of the elements. In 2D triangular and tetrahedral elements, moreover several mesh element size can be chosen and the mesh parameters can be set up. In Fig. 4.15 the finite element mesh of the 2D axial symmetry model can be seen, which contains 34108 triangular elements.

Finally, the problem must be solved. At the *Solver/Solver Parameters...* menu many settings can be set up. Because of the excitation of the above problem is an alternating voltage, the time-harmonic analysis type has been chosen in the upper left corner of the panel. The solution must be calculated for a range of frequencies, i.e. in several value of the frequency, so the parametric solver type has been used. The name of the parameter has been set to $freq$. The parameter values contain the data of the frequency range and the steps in the frequency.

One more task must be done, which is the typing of the parameter $freq$ into the field for *nu_emqa* in the *Physics/Salar Variables...* window. The problem can be solved by a direct solver, such as *UMFPACK* or *SPOOLES*, because the number of the unknowns is

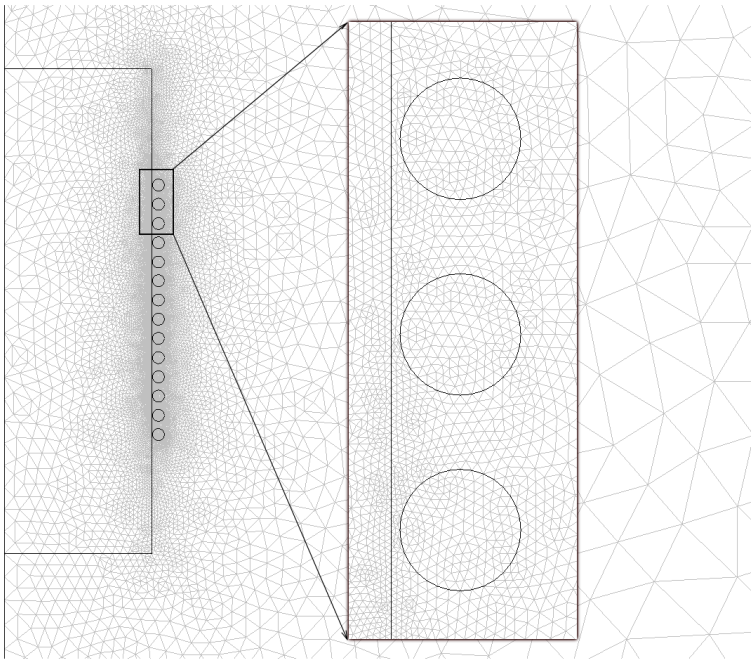

Fig. 4.15. The finite element mesh of the 2D axial symmetry model

not too high, in this case it is 68375. The window of the solver parameters can be seen in Fig. 4.16. In the line *parameter values* `logspace(0,10,20)` means that the problem will be solved in 20 points in the frequency between 10^0 Hz and 10^10 Hz. The distribution of the points are logarithmic.

Optimizing the model

The solution of the above problem provides the results of the unknown quantities via the computed potentials and the calculated integrals and expressions. This is the first chance to check the results and to execute modifications about the model. After the early simulations serious problems were discovered. There are too many finite elements, 59952 in the mesh, which cause 120085 unknowns in the simulation, which made the simulation very slow. The solution time of the problem is 406 secons with a compter having two AMD processor cores and 4 GB ram. The decreasing of the number of mesh elements was necessary. An idea was that the enamel insulation of the winding wire could be neglected, which size is not in the same order of magnitude of the whole model, then the number of the mesh elements could be decreased. To prove the possibility of this modification, two models, with and without the insulation on the winding wire, were compared. The results show that the insulation of the wire can be neglected. Fig. 4.17 shows that the inductance of the inductor simulated with and without insulation are practically the same. After the simplification the solution time decreased to 230 seconds.

An other problem was that the completed model, which is a simplified one, some attributes cannot be simulated, such as the resistance of terminations and the capacitance between the terminations. Because the winding wire is welded to the terminations there are more resistance is appeared, which must be considered. Furthermore, the terminations have large surface, where the charges can crowded, which causes the additional

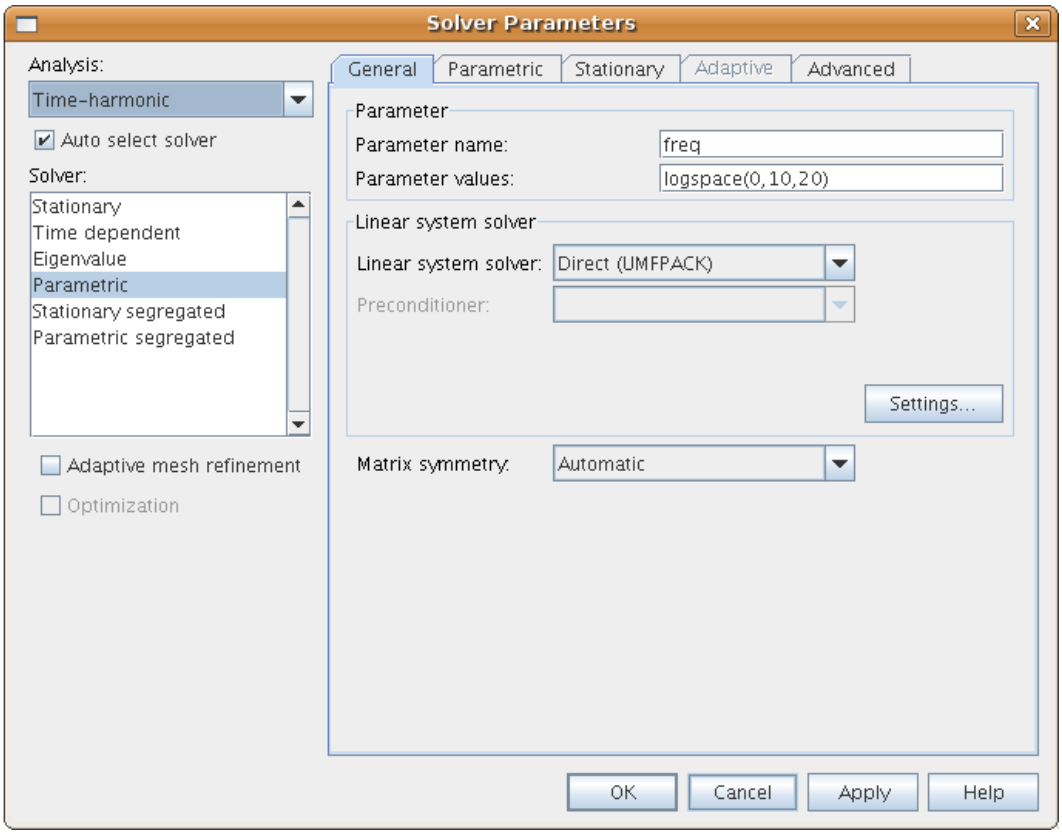

Fig. 4.16. The setting of the solver parameters

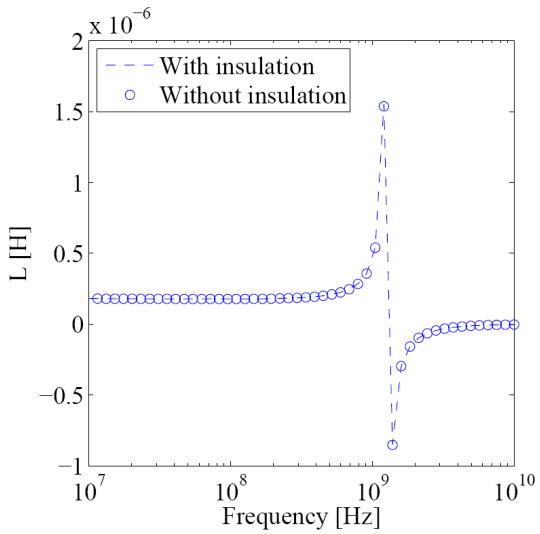

Fig. 4.17. The comparison of the inductance of the inductor simulated with and without insulation on the wire

capacitance.

In the simulation the less resistance and the less capacitance cause higher self-resonant frequency and higher maximum value of the quality factor than the measured one. To compensate these effects, a logical electric network was created, wherein a capacitor and a resistor are in parallel with the simulated inductor to consider the higher capacitance and the higher resistance. In Fig. 4.18 the applied logical electric network can be seen.

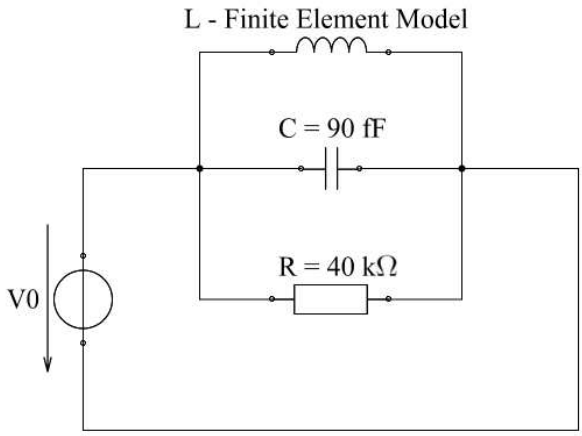

Fig. 4.18. The applied logical network to consider the resistance and the capacitance on the terminations

Our experiences show that the optimal value of the capacitance is 0.09 pF and the value of the resistance is 40 kΩ in the case of this type of inductor. The capacitance is marked C and the resistance is marked $R0$ in Fig. 4.12. The network was built into the finite element model via the modification of the current passing through the component. The modified current is marked Iv in the model. The total current passing through the electric network can be determined by the following formula, henceforth it is used to calculate the impedance and other attributes.

$$I_v = I_{tot} + V_0 \mathrm{j}\omega C + \frac{V_0}{R_0}. \tag{4.6}$$

It is important to note that the components of the network are only parameters, they have not got physical meaning, they just fit the simulated results to the measured data.

Results of the simulation, postprocessing

After building up the finite element model, the computed DC resistance and DC inductance have been compared with analytic calculations and measurement data to check the correctness of the model at low frequencies. The resistance can be got from the following expression :

$$R_{DC} = N\varrho\frac{2r_0\pi}{A}, \tag{4.7}$$

where $r_0 = 0.62$ mm, $N = 14$ and $A = r_c^2\pi = 1.9635\,10^{-9}$ m^2, where r_c is the radius of the wire. Substituting these data to the expression results in 0.463088 Ω. The measured result of the DC resistance is 0.47 Ω. The computed DC resistance can be determined from the real part of the impedance, i.e. $R_{DC} = \mathfrak{Re}\{Z_{DC}\}$, where Z_{DC} is the value of the impedance in direct current case. The computed DC resistance results in 0.485 Ω.

The nominal value of the low frequency inductance is 180 nH of this type of inductor. In a specific case the measured inductance is 183 nH. The computed value of it is 185 nH, which can be determined from the equation

$$L = \frac{\mathfrak{Im}\{\bar{Z}\}}{2\pi f}. \tag{4.8}$$

The analytical expression (2.15) was got from Nagaoka [5]. In this exact case the length of the coil is 1.1 mm and the mean radius of it is 0.62 mm. From Nagaoka's coefficient table $K = 0.6618$ with these dimensions. Substituting this value of K and the actual values of A, N and l to the equation (2.15) leads to the DC inductance of the inductor, which is 178.9 nH. The obtained values are quite close to each other, so it is noticeable, that the created finite element model is working properly at low frequencies.

The comparison of the measured and the computed inductance between 10 MHz and 3 GHz can be seen in Fig. 4.20, and the measured and the computed quality factor can be seen in Fig. 4.19. It can be seen that the results are practically the same, so

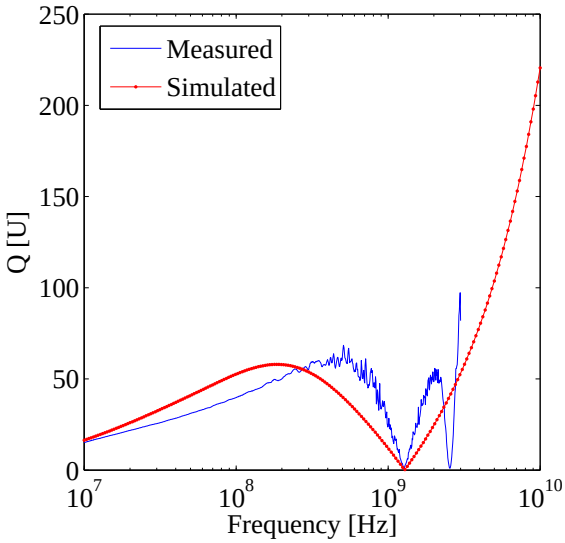

Fig. 4.19. The measured and the computed quality factor

the finite element model is working properly at the whole range of the frequency. The difference between the measured and the computed quality factor is probably caused by the neglecting of the specialities of the core.

At this point, the examination of the modification of the winding was started to find the best geometry of the coil considering the quality factor. Several inductor models, with larger and smaller diameter of the wire, with closely- and widely-spaced coil, and with one and two layered coil was drawn to CAD, the modeling interface of the COMSOL Multiphysics. In Fig. 4.21 finite element meshes of inductors can be seen with three different windings. During the examination finite element models were created and simulated, and trial components were manufactured and measured with the same windings to compare the results.

There are some criteria, which must be fulfilled during designing this type of inductor. First of all, the nominal value of the inductance of the examined component is 180 nH. This value must be kept during the modification. Furthermore, the width of the winding cell, i.e. the space between the terminations, where the coil can be wound, is 1130 μm, so the coil must be fit to there. Because of the manufacturing process, there must be left at least about 10-15 μm space between the turns. If the distance between the turns is smaller, there can be cross-windings in the coil, which worsens the parameters of the inductor. In Fig. 4.22 a cross-winding can be seen on a trial component.

Our experiences show some interesting phenomena, which are observable in the mea-

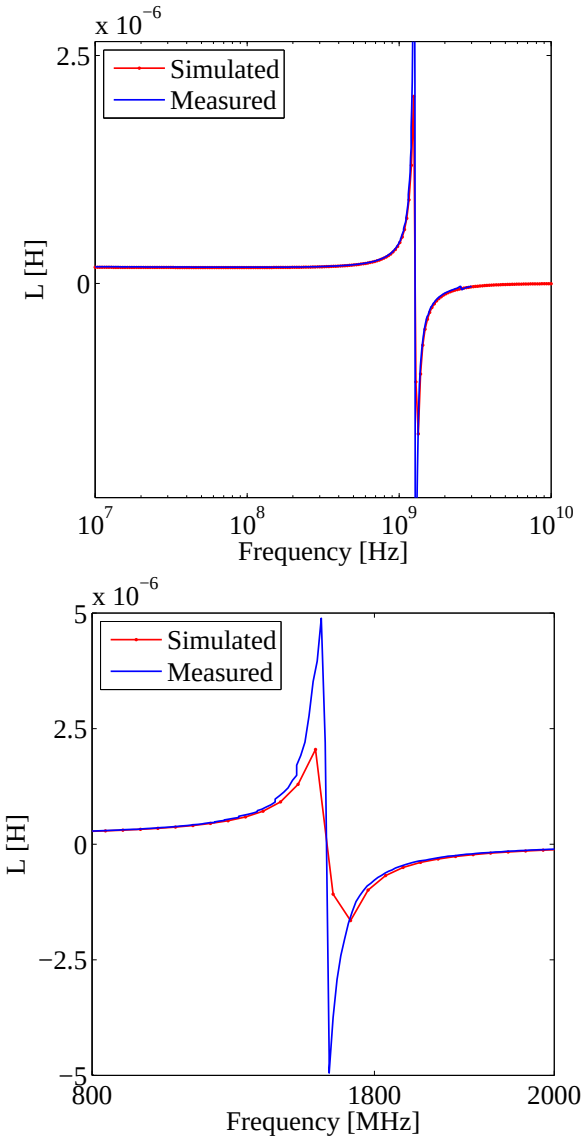

Fig. 4.20. The measured and the computed inductance

surements and the simulations, too. In the first case, the distance between the turns was increased. In the effect of this modification, the value of the inductance was decreased, the SRF was increased through the decreasing the capacitance between the coils, and the maximum value of the quality factor moved to higher frequency, but the value of it was not increased. The decreasing of the distance between the turns effects opposite results. Using a wire with larger diameter causes lower value of the inductance and a wire with smaller diameter effects the opposite result. These phenomena are not too easy to comprehend, but they can be deduced from the works of radio amateurs [4,7,12].

The concrete experiments are the following. It is trivial from the (2.11) that the quality factor will increase if the imaginary part of the impedance increase or the real part of the impedance decreases. Because the nominal value of the inductance must be kept, the solution of the increasing of the Q-factor is the decreasing of the resistance.

The easiest way to decrease the resistance is the using a wire with larger diameter in the coil. So a trial component was manufactured and a finite element model was

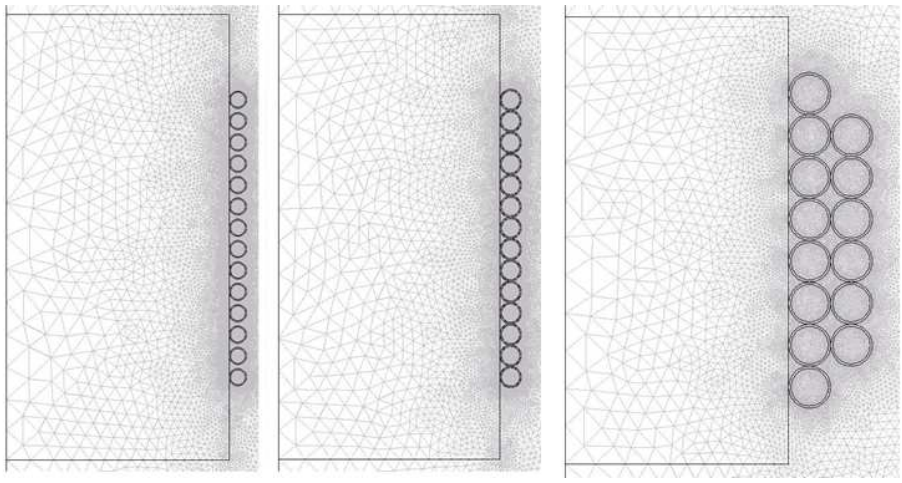

Fig. 4.21. Finite element meshes of three different windings

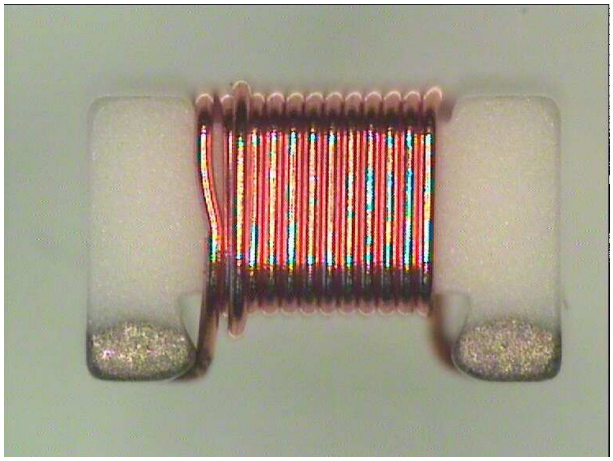

Fig. 4.22. A cross-winding on a trial component

implemented with 60 μm diameter of the winding wire. The results in the simulation showed that the quality factor increase some percents in this case. Unfortunately, in the practice there are some problems. First of all, the measurements show that in the reality the Q is increased slightly than the simulation shows and only at lower frequencies in the studied range. At higher frequencies Q became smaller than in the case of the original wire, but it could not be a problem, because the quality factor has to increase at lower frequencies. Furthermore, because of the manufacturing process the distance between the turns must be increased to eliminate the cross-windings, so the using a wire with larger diameter and the increasing the distance between the turns caused that the value of the inductance is fallen to 170 nH. Because of the width of the winding cell, more turns to compensate the decreasing of the inductance cannot be used. Consequently, it is impossible to increase the quality factor by using thicker wire in the coil.

Then a wire with less diameter, it is 40 μm, was tried. By using thinner wire the value of the inductance is increasing, so it can be enough to wind less turns to the core. Thus, there are more space to "play game" with the wire. During the simulations and the experiments it is cleared that the inductance is not increasing significantly to leave one or more turns. Therefore, 14 turns must also be used in this case. It is executable to spread

the coil on the core, i.e. to increase the distance between the turns, to examine the effect of it. Our experiences show that the SRF is moved to higher frequency, through the less stray capacitance between the turns, and via it the maximum value of the Q-factor is also moved to higher frequency, moreover the maximum value of it is increased slightly. The rise of the quality factor is faster at lower frequencies, but unfortunately it starts to low values. Between 85 and 110 MHz the Q of this trial component is lower than the Q of the present manufactured one. Consequently, the using of thinner wire in the coil is not the solution of the problem. The comparison of the measured and the computed inductance as a function of the frequency and the quality factor of the function of the frequency of the manufactured component and a trial one can be seen in Fig. 4.23 and in Fig. 4.24.

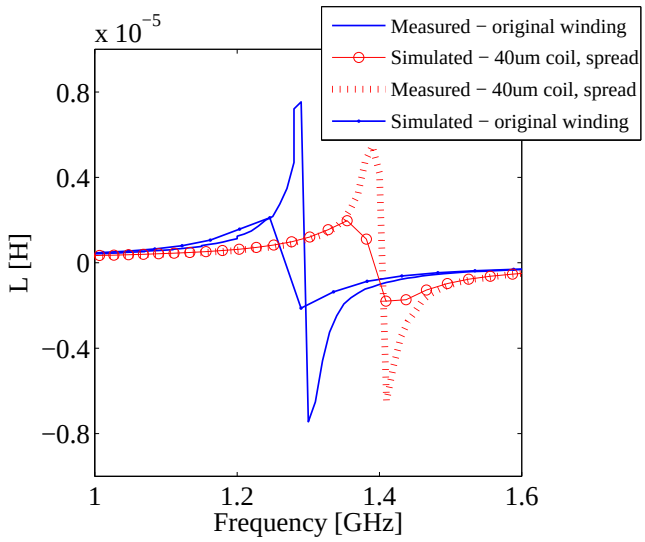

Fig. 4.23. The comparison of the inductance of the manufactured and a trial component

Another attempt was the manufacturing the inductor with ferrite core. Because of the high relative permeability the nominal value of the inductance can be achieved with less turns, which effects the decreasing of the resistance of the coil. The examinations show that it is true, but the quality factor is not increased, moreover it is decreased significantly. The reason of this is the eddy currents and the hysteresis inside the ferrite core, which causes eddy current loss and hysteresis loss. These losses result the lower quality factor of a ferrite cored component. Consequently, manufacturing inductors with ferrite core is not the solution of the problem of the Q-factor.

Finally, we can say that thank to the experiences of the engineers, the presently manufactured component is the best solution of the problem of the quality factor. So, the answer to the first question is that by the modification of the winding the quality factor cannot be increased significantly. But the question is hanging at poise: Is it possible to increase the quality factor, or not? The answer is yes, by the modification of the geometry and by using new materials. The first one is contains several opportunities, moreover it is out of the scope of this work.

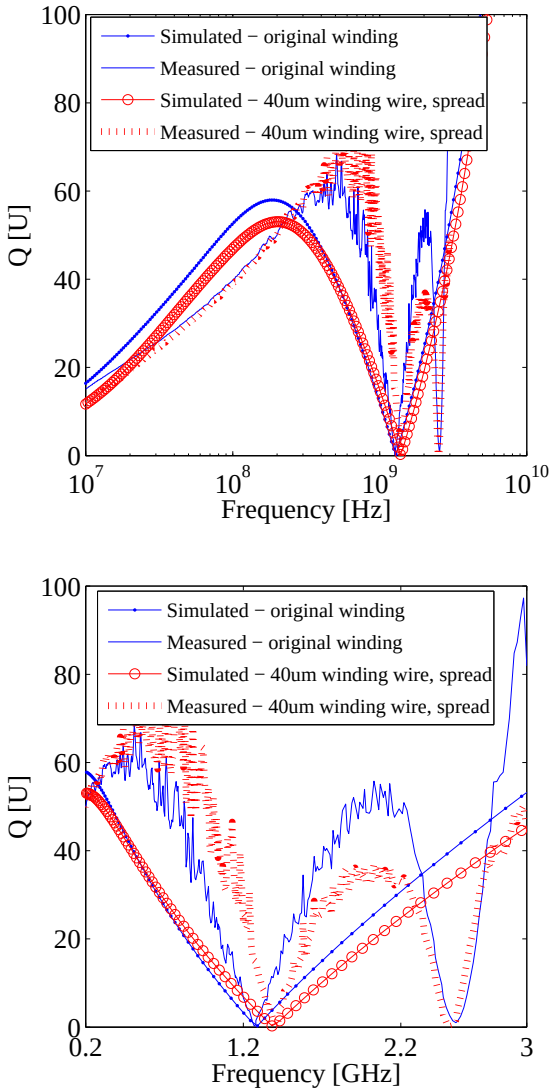

Fig. 4.24. The comparison of the quality factor of the manufactured and a trial component

New materials in the manufacturing

Ferrites using in the present in inductors are soft magnetic materials made of iron (Fe), Nickel (Ni), Zinc (Zn) or Manganese (Mn). Ferrite cores usually have high relative permeability and have close coercive field as it can be seen in Fig. 4.25. It is important to note that the area of the coercive field is proportional to the hysteresis loss of the magnetic material, i.e. which material has closer coercive field, that have less hysteresis loss, so soft magnetic materials are quite good in inductors.

But nowadays there are several researches about making materials better and better. One of these research is about the superparamagnetism. When the size of the particles is reduced below the single domain limit – it is about 15-20 mm for iron oxide –, they exhibit superparamagnetism at room temperature, which means that the magnetic material has high relative permeability, but the area of its coercive field is equal to zero, i.e. it has not got hysteresis loss. The $B - H$ characteristics of a superparamagnetic material is

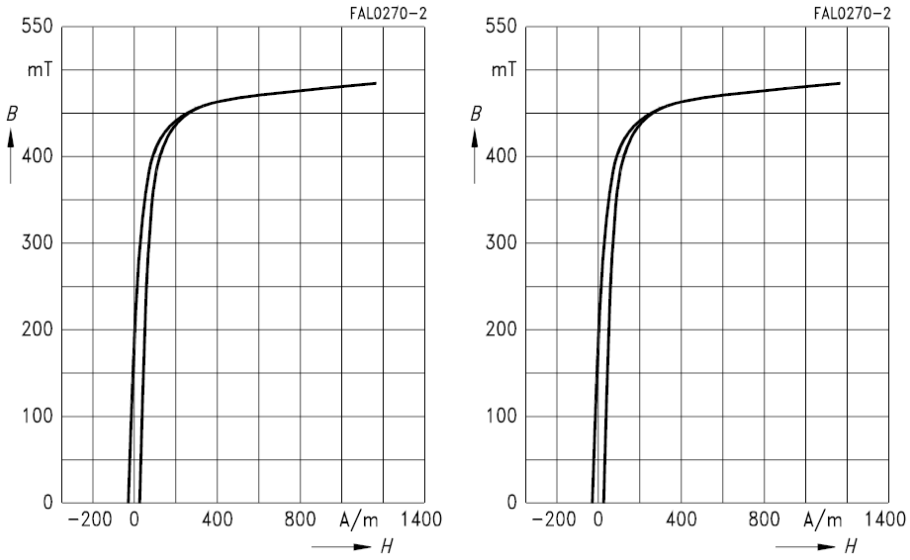

Fig. 4.25. Hysteresis loop of a ferrite core, $f = 10$ kHz, $T_1 = 25$ °C, $T_2 = 100$ °C [26]

an anhysteretic curve. The variation of the coercive field is depend on the size of the particle, as it can be seen in Fig. 4.26. If materials like this could be used in inductors

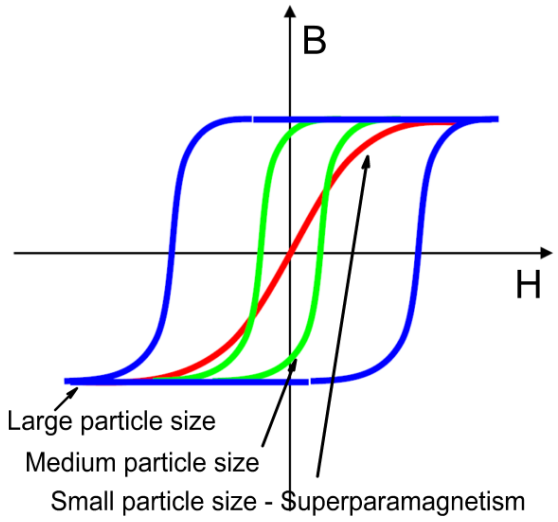

Fig. 4.26. Superparamagnetism

for cores, the quality factor of the component could be increased significantly, because the nominal value of the inductance could be reached with less turns, which means less resistance without losses [31, 33].

Another utopistic way to increase Q of an inductor even more is the discovery of the superconductivity at room temperature and normal pressure, but it also could be a great leap forward if a material could be found, which has higher conductivity than the copper or the silver [35].

4.2 Problem 2: Variation of the Inductance and the Eddy Currents

4.2.1 Overview of the problem

In this section the finite element modeling of an SMT power inductor in the static and in the time dependent cases will be shown. The object of the project is an SMT power inductor named 6x6, manufactured by the EPCOS AG.

There are two different types of this component, a shielded one, which has a ferrite shield on the ferrite core, and an open one. The dimensions of the shielded component are $6.3 \times 6.3 \times 3$ mm, and the dimensions of the open component are $6 \times 6 \times 3$ mm. It has a cylindrical coil from enameled copper wire, which is welded to the terminations. The most important features of the inductor are the wide temperature range tolerance, high current tolerance and the low DC resistance. This type of inductor is usually used to filter supply voltages, coupling, decoupling, in DC/DC converters, in automotive electronics and in industrial electronics. The shielded and the open versions of the inductance can be seen in Fig. 4.27 in microscopic photos.

The aim of these simulations is to determine the variation of the inductance as a function of a manufacturing failure and the orientation of the eddy currents inside the core. The failure is two kind of shifts, when the shield of the component is shifted according to the core vertically or horizontally, because of the imprecision of the manufacturing process. The manufacturer has several experimental experiences about this problem, but it is difficult to find a measuring process to measure the behavior of the variation of the inductance as a function of the shifts. In this case the results can be extrapolated to the whole family of the inductors, so here a specific type of inductor need not to be chosen.

4.2.2 Examination of the effect of the shifts

To model the manufactured components the COMSOL Multiphysics software package has been used again. The three dimensional CAD model of the component was drawn in Pro Engineer by the EPCOS, which was imported to the finite element software. Then the implemented model was modified according to the shifts, which has two types.

In the first case, the axis of the core and the axis of the shield are shifted, but in the second case, the shield is shifted in vertical direction on the core. The inductance of the component was computed in 10 positions of the shield horizontally and in 25 positions vertically. Fig. 4.28 shows the microscopic photo and the finite element mesh of the horizontal shift. In Fig. 4.29 the finite element mesh of the vertical shift can be seen. The setting up of the finite element model was done similarly as it was presented in the past section.

To simulate the above problem, the weak form of the gauged $\boldsymbol{A}$-formulation has been used. In COMSOL Multiphysics there is an opportunity to enter the weak form of partial differential equations. This panel can be found in *Physics/Equation System/Subdomain Settings...* window in the *weak* tab, which can be seen in Fig. 4.30, which shows the Euler form of the weak formulation. The solution of the weak form with the *Conjugate gradients* [36] solver and with the *Algebraic multigrid* [36] preconditioner provides the approximation of the potentials in demand, from which both of the quantities of the studied electromagnetic field and can be determined. The value of the inductance can

Fig. 4.27. The microscopic photo of the inductor

be calculated by the following formula [37]:

$$L = \frac{1}{I^2} \int_\Omega \nu |\nabla \times \boldsymbol{A}|^2 \, \mathrm{d}\Omega, \tag{4.9}$$

where I is the excitation current and $\boldsymbol{A}$ is the magnetic vector potential. The expression can be solved by the built-in integration tool, in the *Postprocessing/Subdomain Inetgration...* menu.

The solution of problem in the both of positions of the shield results the characteristics of the inductance as a function of the shifts. Fig. 4.31 shows the variation of the inductance in the horizontal shift case, and the variation of the inductance in the vertical shift case can be seen in Fig. 4.32. The obtained characteristics can be approximated by polynomial curves. The results of the horizontal shift was described by a cubic curve,

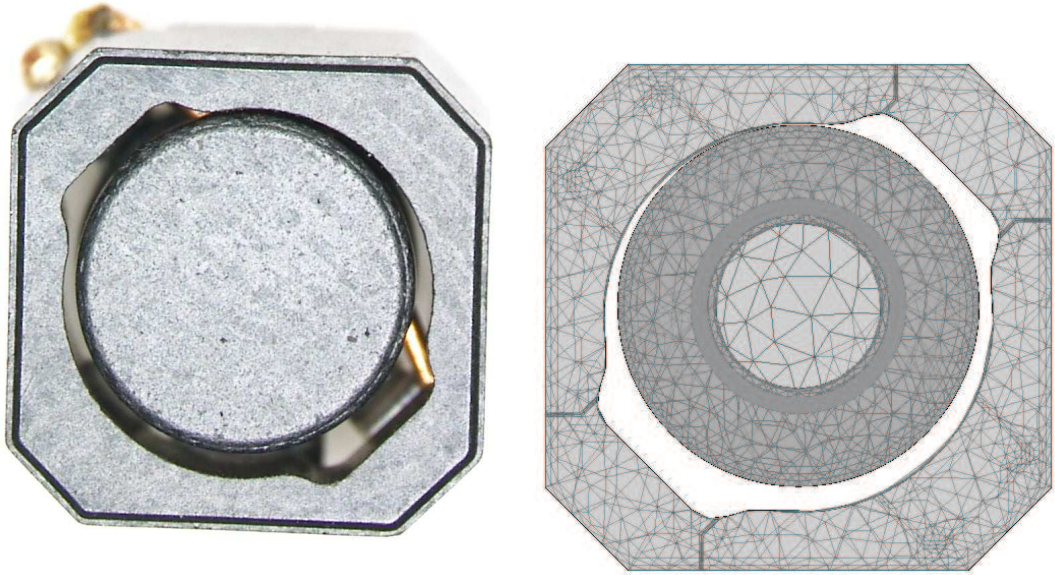

Fig. 4.28. The microscopic photo and the FEM mesh of the horizontal shift

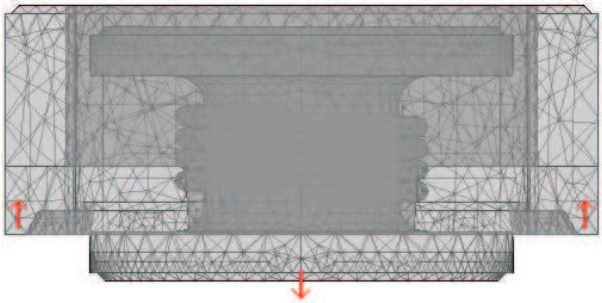

Fig. 4.29. The FEM mesh of the vertical shift

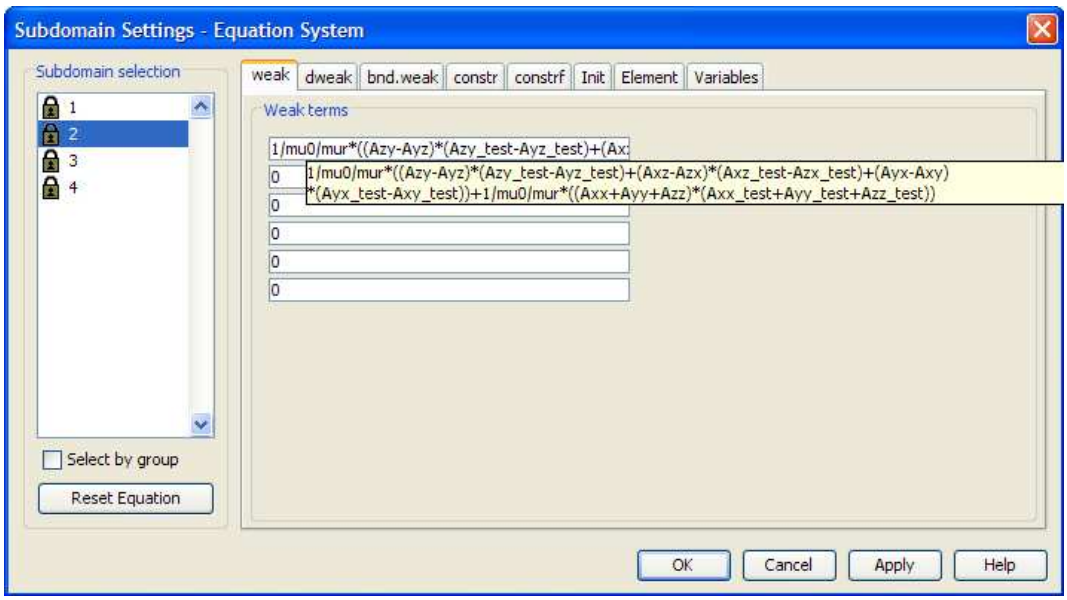

Fig. 4.30. The window where the weak formulation can be entered

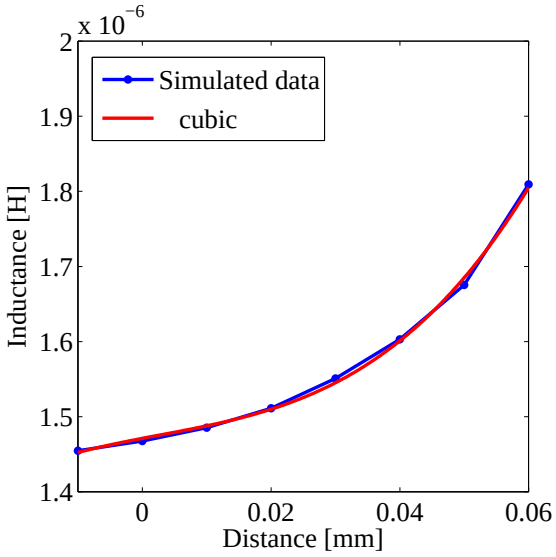

Fig. 4.31. The effect of the horizontal shift to the inductance

which can be described by

$$L(x) = 1.3e^{-9}\,x^3 - 8.6e^{-9}\,x^2 + 3.6^{e-8}\,x + 1.4e^{-6}. \tag{4.10}$$

The characteristics of inductance in the case of the positive vertical shift, as it Fig. 4.29 shows, can be approximated by a linear curve, which is the following,

$$L(x) = -9.7e^{-9}\,x + 1.5e^{-6}. \tag{4.11}$$

In the case of the negative vertical shift, the results can be approximated by a quadratic curve,

$$L(x) = -4.6e^{-10}\,x^2 + 8.4e^{-9}\,x + 1.4e^{-6}. \tag{4.12}$$

Consequently, it can be appointed that in the case of the horizontal shift, the results show that the value of the inductance is increasing while the air gap between the core and the shield is decreasing, because of increasing the flux. In the other case, the inductance is increasing while the core is getting closer and closer to the middle of the shield in vertical direction, else it is decreasing.

4.2.3 Eddy currents inside the core

To determine eddy currents flowing in the core of the inductor, it has been examined as a time dependent magnetic field problem. To solve the problem the weak form of the ungauged $\boldsymbol{A}, V - \boldsymbol{A}$ formulation have been used. The entering of the equations to the COMSOL Multiphysics software can be seen in Fig. 4.33. Because of the numbers of unknowns in the model a direct solver cannot be used, so an iterative one must be applied, which was the GMRES [36]. Eddy currents flowing in the open and the shielded component can be seen in Fig. 4.34. In the open component, blue arrows – marked with $\boldsymbol{J}$ – represents the source current density flowing through the coil of the component.

In Fig. 4.35 the magnetic flux density can be seen in 10 time steps across the core. It seems that by the effect of the eddy currents the flux in the core of the inductor is

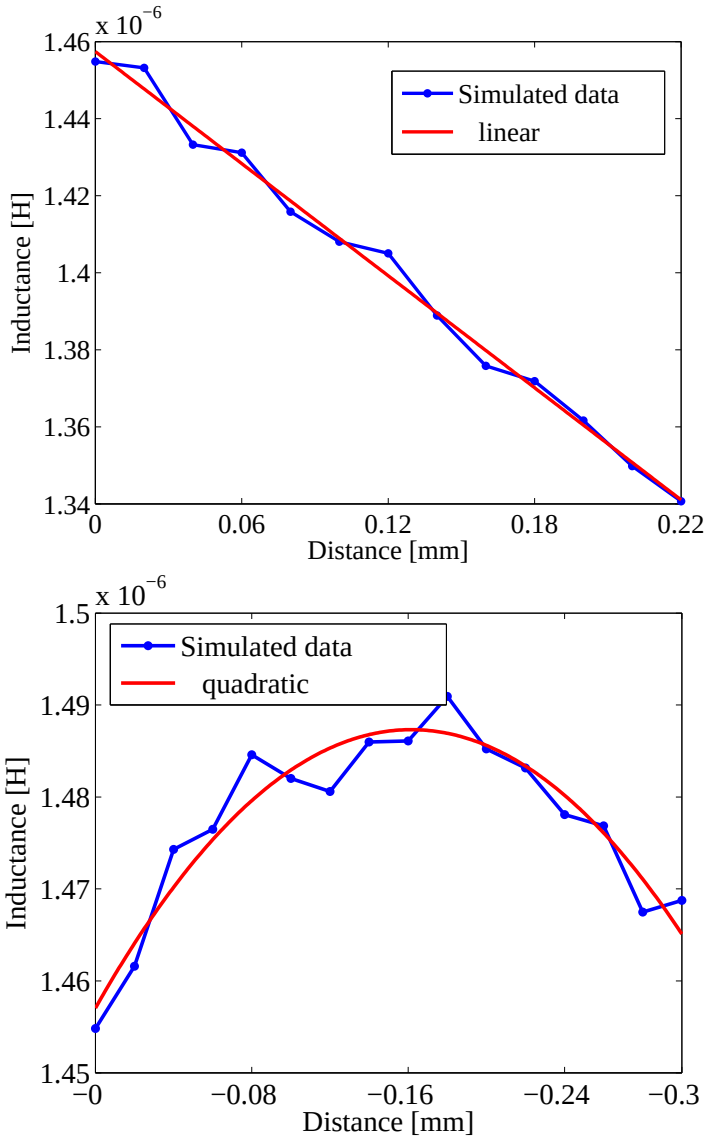

Fig. 4.32. The effect of the vertical shift to the inductance

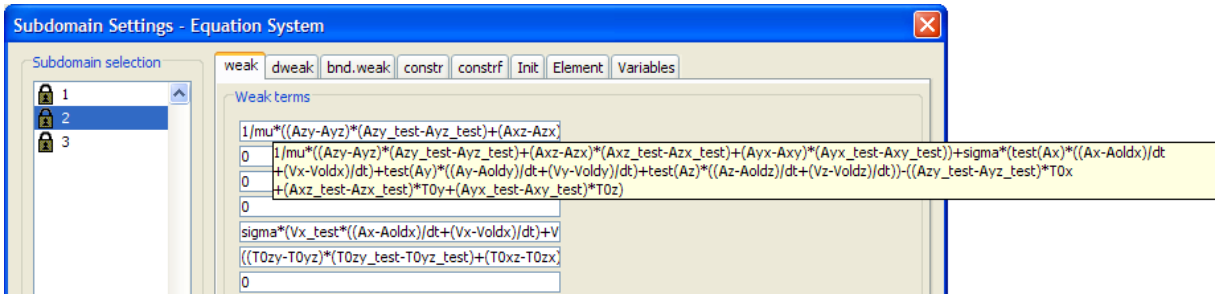

Fig. 4.33. The entering of the weak form of the ungauged $\boldsymbol{A}, V - \boldsymbol{A}$ formulation

decreasing. That causes lower inductance. Moreover eddy currents cause heating in the core, so a part of the invested energy is formed to thermal energy, which decrease the quality factor.

There is only one solution to decrease the effects of the eddy current loss. This way is

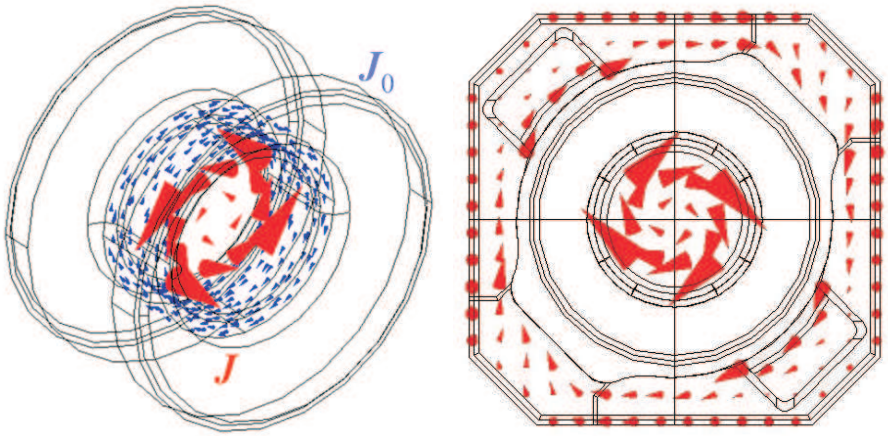

Fig. 4.34. The entering of the weak form of the ungauged $\boldsymbol{A}, V - \boldsymbol{A}$ formulation

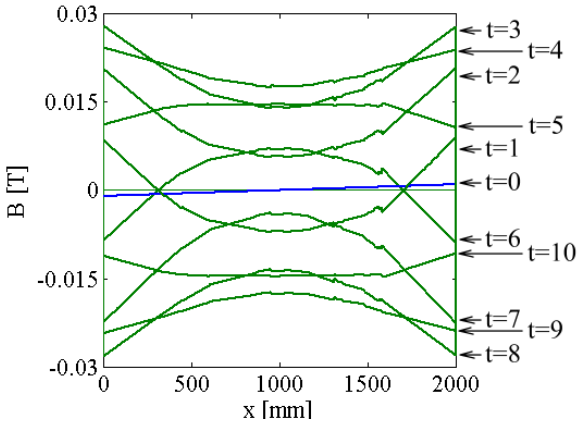

Fig. 4.35. The magnetic flux density modified by eddy currents

to applying new materials for core. For example, nanoparticles with superparamagnetic behavior, presented above, could be applied successfully in the case of this inductor as well.

Chapter 5

Conclusions and Future Work

The paper presents an actual problem of research engineers working with inductors and electronic components. To solve several problems beyond the examination of the quality factor, a finite element model has been developed by using the COMSOL Multiphysics software package.

The weak form of the potential formulations to solve the presented problems has been implemented from the Maxwell's equations. The so-called absorbing boundary condition has been determined and has been applied to eliminate the effect of the reflected electromagnetic waves at the artifical far boundary.

The simulation of the simplified manufactured inductor has been done. To consider the capacitance and the resistance of the terminals, an electric network has been implemented and the values of the parameters have been set to fit the computed results to the measurements. The built up finite element model has been tested. The measurements of the project have been executed in the hungarian factory of EPCOS AG, the results have been described and analyzed. The measured and the analyzed data have been compared with the results of the simulations. Consequently we can say, that by using the present materials and the present manufacturing technology, the quality factor can not be increased significantly, as our experiences show. The increasing of the quality factor can be only realized by applying new materials and new geometries in the manufacturing.

In an other example the variation of the inductance as a function of a manufacturing failure and the orientation of the eddy currents inside the core have been simulated.

The future aim of the project is to simulate the effect of the modification of the geometry of the core to the quality factor, to find out the best geometry considering the quality factor, to simulate the inductor with new material characteristics. In practice we would like to manufacture inductors with improved properties, and if it is possible, we would like to achieve the qualification super high Q in the case of 0805.

Bibliography

[1] Gy. Fodor. *Electromagnetic Fields (in Hungarian).* Műegyetemi Kiadó, 1996.

[2] K. Simonyi and L. Zombory. *Theoretical Electromagnetics (in Hungarian).* Műszaki Könyvkiadó, Budapest, 2000.

[3] O. Heaviside. Electrical Papers. *Macmillan*, p. 429-560. New York, 1892.

[4] F. W. Grover. *Inductance Calculations: Working Formulas and Tables.* Dover Publications, New York, 1946.

[5] H. Nagaoka. *The Inductance Coefficients of Solenoids.* Journal of the College of Science, Imperial University, Tokyo, Japan, 1909.

[6] R. Lundin. A handbook formula for the inductance of a single-layer circular coil. *Proc. IEEE,* Vol. 73, No. 9, Sep. 1985 pp.1428-1429.

[7] R. G. Medhurst. H.F. resistance and self-capacitance of single-layer solenoids. *Wireless Engineer,* Feb. 1947, pp. 35-43, Mar. 1947 pp. 80-92.

[8] E. B. Rosa and F. W. Grover. *Formulas and Tables for the Calculation of Mutual and Self Induction.* Bulletin of the Bureau of Standards, Vol 8, No. 1, Washington, 1911.

[9] K. Kundert. *Modeling Skin Effect in Inductors.* Designer's Guide Community, 2001.

[10] L. Green. *RF-inductor modeling for the 21st century.* EDN, September, 2001.

[11] F. E. Terman. *Radio Engineers' Handbook.* New York, 1943.

[12] D. W. Knight. *Inductors and transformers.* G3YNH, 2001.

[13] O. Martin. *Modeling Non-Ideal Inductors in SPICE.* Newport Components Limited, 1993.

[14] B. K. Sen and R. L. Wheeler. Skin Effects models for Transmission Line Structures using Generic SPICE Circuit Simulators. *Electrical Performance of Electronic Packaging.* 1998.

[15] M. Kuczmann and A. Iványi. *The Finite Element Method in Magnetics.* Akadémiai Kiadó, Budapest, 2008.

[16] O. Bíró and K. R. Richter. CAD in electromagnetism. *in Series Advances in Electronics and Electron Physics, Academic Press, New York,* 82, 1991.

[17] O. Bíró and K. Preis. On the use of the magnetic vector potential in the finite element analysis of three-dimensional eddy currents. *IEEE Trans. on Magn.*, 25:3145-3159, 1989.

[18] O. Bíró, K. Preis, and K. R. Richter. On the use of the magnetic vector potential in the nodal and edge finite element analysis of 3D magnetostatic problems. *IEEE Trans. on Magn.*, 32:651-654, 1996.

[19] O. Bíró. Edge element formulations of eddy current problems. *Comput. Meth. Appl. Mech. Engrg.*, 169:391-405, 1999.

[20] J. Jin. *The Finite Element Method in Electromagnetics.* John Wiley and Sons, New York, 2002.

[21] D. W. Pepper and J. C. Heinrich. *The Finite Element Method.* Taylor and Francis Group, New York, 2006.

[22] W. B. J. Zimmerman. *Multiphysics Modelling with Finite Element Method.* World Scientific Publishing Co., 2006.

[23] I. Bojtár and Zs. Gáspár. *Finite Element Method for Engineers.* TERC, Budapest, 2003.

[24] www.comsol.com

[25] J. D. Jackson. *Classical Electrodynamics.* J. Wiley, New York, 1962.

[26] www.epcos.com

[27] www.agilent.com

[28] www.ceramtec.com

[29] Z. Pólik, M. Kuczmann, Examination and Development of a Radio Frequency Inductor, *Przeglad Elektrotechniczny,* No.12/2008. (under printing).

[30] Z. Pólik, M. Kuczmann, Increasing the Quality Factor of an RF SMT inductor by using the Vector Finite Element Method, *COMPEL,* Volume 28, Number 4, 2009, (under review).

[31] H. Kronmüller and S. Parkin. *Handbook of Magnetism and Advanced Magnetic Materials I.* John Wiley and Sons, 2007.

[32] www.mathworks.com

[33] S. Hariharan and J. Gass. Superparamagnetism and Magneto-caloric Effect (MCE) in Functional Magnetic Nanostructures. *Rev. Adv. Mater. Sci.*, Vol. 10:398-402, 2005.

[34] A. Iványi. *Hysteresis Models in Electromagnetic Computation.* Akadémiai Kiadó, Budapest, 1997.

[35] www.elektrisola.com

[36] P. Kis. *Jiles-Atherton Model Implementation to Edge Finite Element Method.* PhD thesis, Budapest University of Technology and Economics, 2007.

[37] Z. Pólik, M. Kuczmann, Eddy Currents in SMT Inductors Simulated by the Finite Element Method, *Pollack Periodica* (under review).

[38] Comsol. *COMSOL Manual.* COMSOL AB, 2007.

[39] COMSOL. *COMSOL Multiphysics User's Guide.* COMSOL AB, 2007.